

Hydrides: Solid State Transition Metal Complexes

Klaus Yvon & Guillaume Renaudin

Volume III, pp. 1814–1846

in

Encyclopedia of Inorganic Chemistry, Second Edition

(ISBN 0-470-86078-2)

Editor-in-Chief:

R. Bruce King

© John Wiley & Sons, Ltd, Chichester, 2005

Hydrides: Solid State Transition Metal Complexes

Klaus Yvon & Guillaume Renaudin
University of Geneva, Geneva, Switzerland

1	Introduction	1
2	Experimental Details	2
3	Hydride Structure Types and Properties	4
4	Crystal Chemistry	23
5	Properties	28
6	Conclusions	29
7	Related Articles	30
8	References	30

Glossary

Complex metal hydride: solid-state compound containing homoleptic, anionic metal–hydrogen complexes

d^1, d^2, d^3 etc: electron configuration of transition element

ΔH : enthalpy of hydride formation as determined from pressure–composition isotherms during desorption by using van't Hoff's method

Homoleptic hydride complexes: complexes having hydrogen ligands only

Hydrido complexes: structural units formed by central metal atoms and terminal hydrogen ligands

Abbreviations

APW = Augmented plane wave; HT = High temperature; INS = Inelastic neutron scattering, IR = Infrared; lif = Limiting ionic formula; lin = Linear; LCAO-MO = Linear combination of atomic orbitals-molecular orbitals; LT = Low temperature; M = Alkali (Li, Na, K, Rb, Cs), alkaline earth (Mg, Ca, Sr, Ba), divalent (Yb, Eu) or trivalent (La, Nd) lanthanide; NMR = Nuclear magnetic resonance; μ_{eff} = Magnetic moment in units of Bohr magneton, μ_B ; npd = Neutron powder diffraction; oct = Octahedral; pbp = Pentagonal bipyramidal; sad = Saddle-like; spl = Square planar; spy = Square pyramidal; SQUID = Superconducting quantum interference device; T-metal = Transition metal (Mn, Fe, Co, Ni, Cu, Zn, Tc, Ru, Rh, Pd, Cd, Re, Os, Ir, Pt); T_C = Curie temperature; dis = Disordered; tet = Tetrahedral; tri = Triangular; ts = T-shaped; ttp = Tricapped trigonal

prismatic; Z = Number of formula units per crystallographic unit cell.

1 INTRODUCTION

This article is an update of a review written¹ some 10 years ago. It covers the currently known solid-state complex homoleptic transition (T) metal hydrido complexes and some of their properties of interest for science and technology. The complexes occur in a wide variety of solid-state compounds. Historically, the first fully characterized example is K_2ReH_9 . Its structure was reported in 1964 by Abrahams, Ginsberg, and Knox,² and found to contain tricapped trigonal prismatic $[\text{ReH}_9]^{2-}$ complex anions. The second member is Sr_2RuH_6 , which was reported in the 1970s by Moyer and collaborators,³ was found to contain octahedral $[\text{RuH}_6]^{4-}$ complexes. Wider interest in this type of hydride started only in the 1980s after the discovery of ternary transition metal hydrides such as LaNi_5H_6 and FeTiH_2 , which were suitable media for reversible hydrogen storage (for useful reviews see books and journal issues edited by Schlapbach).⁴ The compounds showed metallic properties and had a large homogeneity range with respect to hydrogen. One of them, however, Mg_2NiH_4 , was nonmetallic and had a fixed hydrogen content. Originally reported in 1968 by Reilly and Wiswall,⁵ it was classified as a hydride containing a T-metal hydrido complex only 18 years later, after its structure was fully characterized by Zolliker *et al.*⁶ and found to contain tetrahedral $[\text{NiH}_4]^{4-}$ units called 'complexes'. In the meantime, other homoleptic hydrido complexes were discovered, such as square-pyramidal $[\text{CoH}_5]^{4-}$, square-planar $[\text{PtH}_4]^{2-}$, and linear $[\text{PdH}_2]^{2-}$, and also hydrides that contained both complex bonded hydrogen and ionic hydrogen not bonded to the transition metal. In 1991, some 13 ternary hydride structure types were known. Some of them were reviewed and named 'complex transition metal hydrides' by Bronger,⁷ a term now widely accepted. The first comprehensive review as written in 1993 by Yvon¹ covered 25 different transition metal hydride complexes in some 69 compounds, including quaternary hydrides. Over the years, the number of complex metal hydrides increased continuously and reviews appeared on various of their aspects such as synthetics,^{8,9} diffraction methodology,^{10,11} bonding,¹²⁻¹⁴ crystal chemistry,^{15,16} complex formation in hydrogenated intermetallic compounds,¹⁷ and materials science.^{18,19} The hydrides were also incorporated into a public online database.²⁰ At present, over 127 complex T-metal hydrides covering 47 structure types are known, that is, since the 1993 review their number has almost doubled. In this update, both mononuclear (terminal hydrogen ligands only) and polynuclear (terminal and bridging hydrogen ligands)

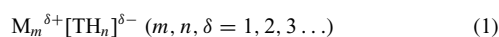
complexes are covered. Only those hydrides are treated whose structures are fully characterized. Most contain well-defined T-metal hydride complexes and show nonmetallic behavior. Some, however, do not, and their classification as ‘complex’ hydrides is debatable. They are, nevertheless, included here because they illustrate the continuous transition that exists between complex and interstitial (metallic) hydrides. Among the aspects discussed are factors that govern the formation of complex hydrides, hydrogen contents, and thermal stability. These factors are not only of fundamental interest but also of practical relevance, because they determine the potential of metal hydrides for hydrogen storage applications.

2 EXPERIMENTAL DETAILS

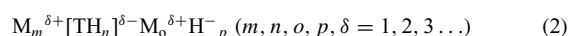
2.1 Compositions and Structures

The presently known complex transition metal hydrides are based on late 3d, 4d, and 5d transition elements of groups 7–10, and on monovalent, divalent, and trivalent metals (M) belonging to the alkali, alkaline earth, and/or lanthanide series, respectively. For completeness, complexes based on closed-shell elements of group 11 (Cu, etc.) and 12 (Zn, etc.) are also included. Most hydrides are true ternary (or quaternary) compounds in the sense that they do not derive from stable intermetallic compounds, but form only in the presence of hydrogen. Some hydrides, however, do and show interesting physical phenomena. The metal ratios are usually situated in the range $M/T = 1-4$, and the hydrogen contents in the range $H/(M + T) = 1-4.5$. The compounds crystallize with 47 different, mostly new, structure types and represent over 127 hydrides. The first representative of each hydride structure type and the isostructural compounds known are listed in chronological order in Table 1 (year of publication in parentheses).

There exist two broad families of complex transition metal hydrides. The first contains hydrogen bonded to transition elements only and has the general composition



where $[TH_n]^{\delta-}$ are complexes that are stabilized by charge transfer from the surrounding metal cations $M^{\delta+}$. The second family contains hydrogen bonded to T elements and hydride anions H^- bonded to metal cations $M^{\delta+}$ only, corresponding to the general composition



These ‘composite’ hydrides are of particular interest because they combine different types of metal–hydrogen bonding in the same structure.

Table 1 Complex transition metal hydride structure types and representatives

Structure types	Representatives	Complex transition metal hydrides
I	K ₂ ReH ₉ (1964)	K ₂ TH ₉ (T = Tc, Re)
II	Sr ₂ RuH ₆ (1971)	M ₂ FeH ₆ (M = Mg, Ca, Sr, Eu, Yb) M ₂ RuH ₆ (M = Mg, Ca, Sr, Ba, Eu, Yb) M ₂ OsH ₆ (M = Mg, Ca, Sr, Ba) M ₂ PtH ₆ (M = Na, K, Rb, Cs)
III	Sr ₂ IrH ₅ (1971)	Mg ₂ CoH ₅ M ₂ RhH _{5+x} (M = Ca, Sr, Eu) M ₂ IrH _{5+x} (M = Mg, Ca, Sr, Eu)
IV	Na ₂ PtH ₄ (1984)	M ₂ PdH ₄ (M = Na, K) Na ₂ PtH ₄
V	Mg ₂ NiH ₄ (1986)	Mg ₂ NiH ₄
VI	K ₂ PtH ₄ (1986)	M ₂ PdH ₄ (M = Rb, Cs) M ₂ PtH ₄ (M = K, Rb, Cs)
VII	Na ₂ PdH ₂ (1988)	M ₂ PdH ₂ (M = Li, Na)
VIII	K ₃ PtH ₅ (1988)	M ₃ TH ₅ (M = K, Rb, Cs and T = Pd, Pt)
IX	K ₃ PdH ₃ (1990)	M ₃ PdH ₃ (M = K, Rb, Cs)
X	CaPdH ₂ (1990)	MPdH _{3-x} (M = Ca, Sr, Eu, Yb) MNiH _{3-x} (M = Ca, Yb)
XI	Li ₄ RuH ₆ (1991)	M ₄ RuH ₆ (M = Li, Na) Li ₄ OsH ₆
XII	Na ₃ RhH ₆ (1991)	M ₃ TH ₆ (M = Li, Na and T = Rh, Ir)
XIII	Li ₃ RhH ₄ (1991)	Li ₃ RhH ₄
XIV	MgRhH _{1-x} (1992)	MgRhH _{0.94}
XV	Mg ₃ RuH ₃ (1992)	Mg ₃ RuH ₃
XVI	SrMg ₂ FeH ₈ (1992)	MMg ₂ FeH ₈ (M = Sr, Ba, Eu)
XVII	Mg ₆ Co ₂ H ₁₁ (1992)	Mg ₆ Co ₂ H ₁₁
XVIII	Mg ₂ RuH ₄ (1992)	Mg ₂ RuH ₄
XIX	CaMgNiH ₄ (1992)	MMgNiH ₄ (M = Ca, Sr, Eu, Yb)
XX	Ca ₄ Mg ₄ Fe ₃ H ₂₂ (1992)	M ₄ Mg ₄ Fe ₃ H ₂₂ (M = Ca, Yb)
XXI	Ba ₂ PtH ₆ (1993)	M ₂ PtH ₆ (M = Sr, Ba)
XXII	LiSr ₂ PdH ₅ (1993)	LiSr ₂ PdH ₅
XXIII	Mg ₃ ReH ₇ (1993)	Mg ₃ TH ₇ (T = Mn, Re)
XXIV	Mg ₄ IrH ₅ (1993)	Mg ₄ IrH ₅
XXV	Mg ₃ RuH ₆ (1993)	Mg ₃ RuH ₆
XXVI	Sr ₈ Rh ₅ H ₂₃ (1994)	M ₈ Rh ₅ H ₂₃ (M = Ca, Sr)
XXVII	LiMg ₂ RuH ₇ (1994)	LiMg ₂ TH ₇ (T = Ru, Os)
XXVIII	BaReH ₉ (1994)	BaReH ₉
XXIX	K ₂ ZnH ₄ (1994)	M ₂ ZnH ₄ (M = K, Rb, Cs) M ₂ PdH ₄ (M = Sr, Ba, Eu)
XXX	K ₃ ZnH ₅ (1994)	M ₃ TH ₅ (M = K, Rb, Cs and T = Mn, Zn) Cs ₃ CdH ₅
XXXI	Ba ₃ Ir ₂ H ₁₂ (1994)	Ba ₃ Ir ₂ H ₁₂
XXXII	Ca ₄ Mg ₄ Co ₃ H ₁₉ (1995)	M ₄ Mg ₄ Co ₃ H ₁₉ (M = Ca, Yb)
XXXIII	KNaReH ₉ (1995)	KNaReH ₉
XXXIV	Li ₅ Pt ₂ H ₉ (1995)	Li ₅ Pt ₂ H ₉
XXXV	Ba ₇ Cu ₃ H ₁₇ (1996)	Ba ₇ Cu ₃ H ₁₇
XXXVI	LiMg ₄ Os ₂ H ₁₃ (1996)	LiMg ₄ T ₂ H ₁₃ (T = Ru, Os)
XXXVII	Li ₂ PtH ₂ (1996)	Li ₂ PtH ₂
XXXVIII	BaMg ₂ RuH ₈ (1997)	BaMg ₂ TH ₈ (T = Ru, Os)
XXXIX	NaBaPdH ₃ (1998)	NaBaPdH ₃

Table 1 cont'd

Structure types	Representatives	Complex transition metal hydrides
XL	K ₃ ReH ₆ (1998)	K ₃ ReH ₆
XLI	Ca ₈ Rh ₆ H ₂₄ (1998)	Ca ₈ Rh ₆ H ₂₄
XLII	Rb ₃ ReH ₁₀ (1998)	M ₃ ReH ₁₀ (M = K, Rb, Cs)
XLIII	Na ₃ OsH ₇ (2002)	Na ₃ TH ₇ (T = Ru, Os)
XLIV	Cs ₃ OsH ₉ (2002)	M ₃ OsH ₉ (M = Rb, Cs)
XLV	Mg ₆ Ir ₂ H ₁₁ (2002)	Mg ₆ Ir ₂ H ₁₁
XLVI	NdMgNi ₄ H ₄ (2003)	MMgNi ₄ H _{~4} (M = La, Nd)
XLVII	LaMg ₂ NiH ₇ (2003)	LaMg ₂ NiH ₇

2.2 Synthesis

The most common route of synthesis is by solid-state reaction, such as sintering powder mixtures of the elements, binary alloys, and/or binary metal hydrides at relatively high pressures (up to 160 bar) and moderate temperatures (<1000 K). Synthesis from binary metal compounds is rarely possible because such compounds either do not exist, such as in the Mg–Fe and Mg–Os systems, or form at metal ratios that differ significantly from those of the ternary (or quaternary) complex metal hydrides, such as Mg₂CoH₅ (MgCo, MgCo₂) or Mg₂RuH₆ (Mg₃Ru₂). Some hydrides derive from two-phase mixtures such as Ba₇Cu₃H₁₇ (Ba–Cu alloy with compositional ratio Ba/Cu~7/3) while others can be prepared by inexpensive ball milling (Mg₂FeH₆) and combustion synthesis (Mg₂NiH₄). Solution methods, such as those employed to synthesize K₂ReH₉ and related hydrides, are not yet fully explored. The only other soluble T-metal hydride complex known is [FeH₆]⁴⁻.²¹ The solid-state reaction products are mostly polycrystalline and often colored. They usually contain impurity phases (nonreacted T and/or binary M metal hydrides), but rarely contain single crystals of sufficient size and quality for diffraction measurements or measurements of physical properties. Those based on alkali and heavy alkaline earth metals are often sensitive to air and moisture.

A decisive parameter for hydride formation is pressure. The synthesis of hydrides based on light transition elements usually requires higher hydrogen pressures than those based on heavier congeners. Examples are the palladium compounds M₂PdH₄ and M₃PdH₅, which form at 20 and 70 bar, respectively, in contrast to their platinum congeners, that form already at 1 bar. For a given transition metal, an increase of hydrogen pressure usually allows the stabilization of higher formal oxidation states. Examples are found for palladium in M₃Pd⁰H₃ and M₂Pd^{II}H₄, which form at 1 and 20 bar, respectively, for platinum in K₂Pt^{II}H₄ and K₂Pt^{IV}H₆, which form at 1 and 1800 bar respectively, and for ruthenium in Mg₂Ru⁰H₄ and Mg₂Ru^{II}H₆, which form at 20 and 90 bar, respectively. However, the inverse situation prevails for manganese based Mg₃Mn^IH₇, which forms under a mechanical pressure of

20 kbar, while K₃Mn^{II}H₅ forms under a hydrogen gas pressure of only 3 kbar.

2.3 Structure Analysis

Owing to the low X-ray scattering power of hydrogen, neutron diffraction experiments on deuterides are necessary. Most atomic arrangements are determined on powders, and this may cause difficulties owing to poor crystallinity, the presence of impurity phases (often not detected by X rays), structural complexity (Mg₆Ir₂D₁₁, e.g., has 126 free positional parameters), heavy absorption (Eu, Cd), microtwinning owing to temperature induced phase transitions, and disorder in the hydrogen complex ligand spheres. High-resolution measurements (e.g. with synchrotron radiation) are rare. The data are usually analyzed by the Rietveld method. For better convergence, the number of refined parameters, in particular, those of the atomic displacement amplitudes, are reduced by constraints. For all these reasons, hydride structures are generally less well characterized than other solid-state structures.

2.4 Properties

Most compounds are nonmetallic. Only few other properties are known. The main reason for this is the lack of single crystals, the presence of impurity phases in the samples, and the sensitivity of many compounds to air and moisture. Data on magnetic, electric, and spectroscopic (NMR, Mössbauer, IR) properties are scarce. Enthalpies of hydride formation as measured from pressure–composition isotherms are known for hydrides based on 3d elements only. Theoretical band structure calculations are available only on relatively simple crystal structures. Structural dynamics are investigated by spectroscopic methods (INS, Raman, IR, NMR) and magnetic properties on SQUID magnetometers. Owing to the absence of single crystals of suitable size, reliable measurements of the electric conductivity are rare. Enthalpies of hydride formation, ΔH , are usually determined from pressure–composition isotherms as measured on Sievert's apparatus or on a thermobalance, by using the relation

$$\ln(p_{\text{eq}}) = \frac{-\Delta H}{R.T} + \frac{\Delta S}{R} \quad \text{Van't Hoff equation} \quad (3)$$

where p_{eq} is the hydrogen equilibrium pressure and T the absolute temperature. Given that the entropy term, ΔS , does not much change from one system to another ($\Delta S \sim 130 \text{ J K}^{-1} \text{ mol}^{-1} \text{ H}_2$) the hydrogen decomposition temperatures at a given pressure scale roughly with enthalpy (293 K: $\Delta H \sim 30 \text{ kJ/H}_2$ for $p_{\text{eq}} = 1 \text{ bar}$). Finally, the reaction products ought to be handled with care because many are air sensitive and some are extremely pyrophoric. For these reasons, quite a few complex metal hydrides are known to exist but have not yet been fully characterized.

3 HYDRIDE STRUCTURE TYPES AND PROPERTIES

Complex transition metal hydrides combine structural features typical for coordination compounds and ionic solids. They display covalently bonded hydrogen such as in molecular transition metal complexes²² (see *Hydride Complexes of the Transition Metals*), and hydride anions (H^-) bonded to electropositive metals (M^+ , M^{2+} , M^{3+}) only, such as in saline hydrides. In metal-rich systems, hydrogen has interstitial character, as in typically metallic transition metal hydrides.²³ The structural and physical properties of the 47 known hydride structure types and of their representatives (stated in parentheses) are summarized below. Limiting ionic formulas (lif) and the corresponding formal oxidation states and electron configurations of the transition elements are indicated whenever possible. Such formulas do not provide an adequate description of the bonding but allow one to rationalize the H content (see below). For each structure, T–D bond distances and shortest M–D (complex D), M–D⁻ (anionic D⁻) and D–D distances are stated. For all structure types, illustrations are given (see Figures 1–47; TH_n complexes are drawn by heavy lines, disordered ligands by double lines, M–M contacts surrounding TH_n complexes by single lines, M atoms as large circles, and H^- ions as small isolated circles).

3.1 K_2ReH_9 (K_2TcH_9)

From reaction of $KReO_4$ with K metal in ethylenediamine–water solution;² colorless crystals, unstable in moist air; NMR and IR data, optical absorption spectra and LCAO–MO calculations; ordered structure (Figure 1) from single-crystal neutron diffraction on hydride and later on deuteride:²⁴ $P\bar{6}2m$, $Z = 3$; two different Re sites, occurring at the ratio Re1:Re2 = 1:2, both forming $ttp-[ReH_9]^{2-}$ 18-electron complexes with T site symmetries $\bar{6}2m$ and $\bar{6}$, respectively; surrounded by two types of K cations; four H sites; lif: $2K^+ \cdot [ReH_9]^{2-}$; Re^{VII} , d^0 ; no structure data on Tc compound.

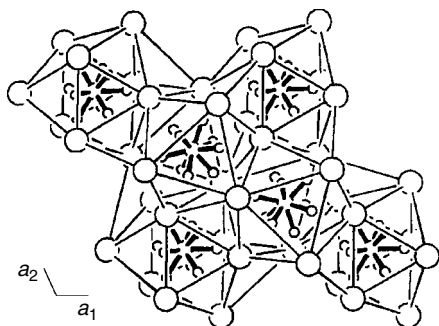


Figure 1 Structure of K_2ReH_9

Distances (\AA):²⁴ Re–H ($3\times$) = 1.68 (Re1); 1.67 (Re2); Re–H ($6\times$) = 1.69 (Re1); 1.70 (Re2); K–H = 2.69; H–H = 1.90.

3.2 Sr_2RuH_6 (M_2FeH_6 , $M = Mg, Ca, Sr, Yb, Eu$; M_2RuH_6 , $M = \text{any}$; M_2OsH_6 , $M = Mg, Ca, Sr, Ba$; M_2PtH_6 , $M = Na, K, Rb, Cs$)

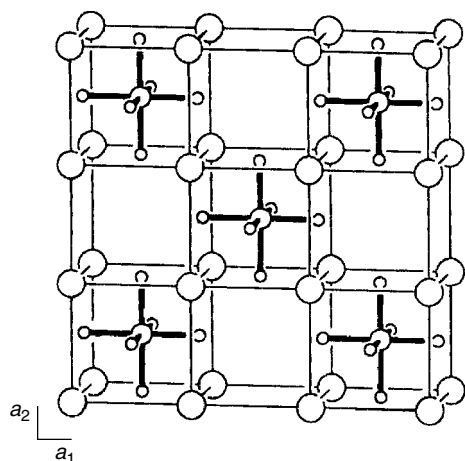
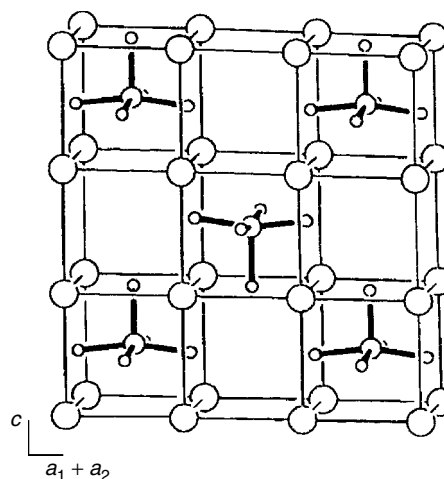
Sr_2RuH_6 and isostructural hydrides M_2TH_6 from elemental T (Fe, Ru, Os) and binary hydrides MH_2 or Mg by sintering at various temperatures and hydrogen pressures;^{3,25–30} or by mechanical alloying followed by sintering ($T = Fe$);^{31,32} powders either colored (Mg_2FeH_6 , green; Eu_2RuH_6 , red), or white-gray (Ca_2RuH_6 , Mg_2OsH_6), or black (Yb_2RuH_6); moisture sensitive and partly pyrophoric (Mg_2OsH_6); M_2FeH_6 ($M = Ca, Sr, Eu$), M_2OsH_6 ($M = Mg, Ca$), Mg_2RuH_6 and various solid solutions;²⁹ M_2PtH_6 ($M = Na, K, Rb, Cs$)^{33–35} by reaction of alkaline hydride with platinum sponge at 770 K under high hydrogen pressure (between 2 and 4 kbar); M_2PtH_6 are colorless and very sensitive to moisture and air; IR stretching frequencies of T–H ($T = Fe, Ru, Os$) bonds range between 1450 and 1850 cm^{-1} , and increase in the sequence Fe, Ru, Os, and decrease as the ionic size of M^{2+} increases;²⁸ Eu_2RuH_6 and solid solution series (Ca, Eu) $_2RuH_6$ and (Sr, Eu) $_2RuH_6$ are paramagnetic with $\mu_{eff} = 7.7\mu_B$, and magnetic order below $T_C = 29 K$;²⁵ low-temperature magnetic properties of $Eu-Ru$, (Ca, Eu)– Ru , and (Sr, Eu)– Ru hydrides³⁶ show ferromagnetic behavior; electric resistivities of Mg_2FeH_6 , Ca_2RuH_6 , Sr_2RuH_6 , Yb_2RuH_6 , and Eu_2RuH_6 indicate nonmetallic behavior; band structure calculations³⁷ predict band gaps that range from 1.3 eV (Sr_2FeH_6) to 4.0 eV (Mg_2OsH_6) and increase in the sequence Mg_2TH_6 ($T = Fe, Ru, Os$) and decrease in the sequence M_2FeH_6 ($M = Mg, Ca, Sr$); Mg_2FeH_6 , Ca_2RuH_6 , Sr_2RuH_6 are diamagnetic, or weakly paramagnetic; other properties of Mg_2FeH_6 : Mössbauer spectra²⁶ consistent with low-spin Fe^{II} ; hydrogen density 5.4 wt%; 9.0×10^{22} H atoms cm^{-3} ; desorption enthalpy²⁶ $\Delta H = 98 kJ mol^{-1} H_2$; INS, infrared, and Raman spectroscopies;³⁸ has potential for thermochemical thermal energy storage;³⁹ IR of Ru based hydrides;⁴⁰ ordered structures (Figure 2) by npd on deuterides;^{3,26–29} $Fm\bar{3}m$, $Z = 4$; K_2PtCl_6 type structure; octahedral $[TH_6]^{4-}$ 18-electron complexes having T site symmetry $m\bar{3}m$; surrounded by M in eightfold cubic configuration corresponding to a CaF_2 type metal substructure; lif: $2M^{2+} \cdot [TH_6]^{4-}$; $T = Fe^{II}$, Ru^{II} , Os^{II} ; d^6 . Interatomic distances are given in Table 2.

3.3 Sr_2IrH_5 (Mg_2CoH_5 , Mg_2IrH_5 , Ca_2IrH_5 , $Ca_2RhH_{5.4}$, $Sr_2RhH_{5.3}$, Eu_2IrH_5)

Sr_2IrH_5 from Ir and SrH_2 powder at 1033 K under hydrogen;⁴¹ Eu_2IrD_5 from ¹⁵³Eu isotope enriched intermetallic $EuIr_2$ at 673 K under deuterium,⁴² or by reaction of binary europium hydride (natural isotope mixture) with iridium metal

Table 2 Interatomic distances (Å) in Sr_2RuD_6 and analogs

		T = Fe	T = Ru	T = Os			T = Pt
M = Mg	T-D	1.56	1.67	1.68	M = Na	T-D	1.62
	T-Mg	2.79	2.87	2.89		T-Na	3.18
	Mg-D	2.28	2.34	2.36		Na-D	2.60
	Mg-Mg	3.22	3.31	3.34		Na-Na	3.67
	D-D	2.20	2.32	2.34		D-D	2.28
M = Ca	T-D	1.62		1.73	M = K	T-D	1.64
	T-Ca	3.05		3.14		T-K	3.62
	Ca-D	2.49		2.57		K-D	2.90
	Ca-Ca	3.52		3.63		K-K	4.07
	D-D	2.29		2.45		D-D	2.32
M = Sr	T-D		1.69		M = Rb	T-D	1.63
	T-Sr		3.29			T-Rb	3.70
	Sr-D		2.69			Rb-D	3.06
	Sr-Sr		3.80			Rb-Rb	4.27
	D-D		2.40			D-D	2.30
M = Ba	T-D		1.72	1.78	M = Cs	T-D	1.64
	T-Ba		3.47	3.48		T-Cs	3.88
	Ba-D		2.85	2.85		Cs-D	3.23
	Ba-Ba		4.01	4.02		Cs-Cs	4.48
	D-D		2.44	2.51		D-D	2.32

**Figure 2** Structure of Sr_2RuD_6 **Figure 3** Structure of Mg_2CoD_5

at 970 K under deuterium pressure;⁴³ Mg_2CoH_5 by sintering metal powder mixtures at 620–770 K under 40–60 bar hydrogen pressure;⁴⁴ or by mechanical alloying followed by sintering;³¹ properties of Mg_2CoH_5 : black powder; electric resistivity consistent with nonmetallic behavior; band structure calculations³⁷ predict band gap of 1.9 eV, magnetization measurements indicate weak paramagnetism (possibly diamagnetism); ordered structure (Figure 3) from npd:⁴⁴ $P4/nmm$, $c/a = 1.477$; $Z = 1$; square-pyramidal $[\text{CoH}_5]^{4-}$ 18-electron complex with T site symmetry $4mm$; surrounded by two Mg sites in eightfold nearly cubic configuration; two D sites, both ordered; transforms at 488 K into disordered cubic HT (high temperature) modification

similar to II; lif: $2\text{Mg}^{2+} \cdot [\text{CoH}_5]^{4-}$; Co^1 ; d^8 ; H distribution in presumably isostructural Mg_2IrH_5 not yet confirmed; hydrogen density: 4.5 wt%, 7.5×10^{22} H atoms cm^{-3} ; desorption enthalpy $\Delta H = 86 \text{ kJ mol}^{-1} \text{ H}_2$; decomposes into $\delta\text{-MgCo}$ and MgH_2 ;⁴⁵ Sr_2IrD_5 : partially disordered structure from npd⁴¹ at 4.2 K: $I4/mmm$, $c/a = 1.465$, $Z = 2$; Ir surrounded by five D in a partially disordered average octahedral configuration having $4/mmm$ site symmetry; equatorial D sites fully and apical D sites half occupied; transforms between 140 and 200 K into disordered cubic HT modification similar to II; $\text{Ca}_2\text{RhD}_{5.4}$ and $\text{Sr}_2\text{RhD}_{5.3}$ with higher occupancy factor 0.89(2),^{46,47} disordered cubic structure by npd: $Fm\bar{3}m$, $Z = 4$, no phase transition; Eu_2IrD_5 ,

Table 3 Interatomic distances (Å) in Sr₂IrD₅ and analogs

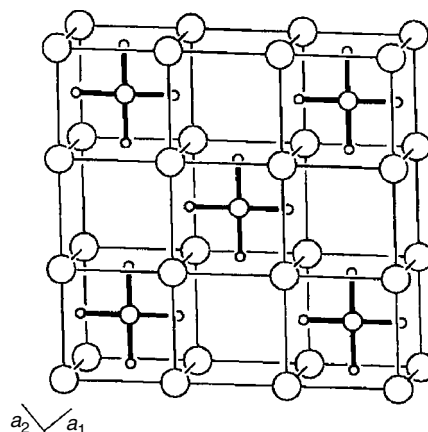
		Cubic HT-phases			Tetragonal LT-phases		
		T = Co	T = Rh	T = Ir	T = Co	T = Rh	T = Ir
M = Mg	T-D	1.53			(4×)1.51 (1×)1.59		
	T-Mg	2.79			2.75		
	Mg-D	2.28			2.23		
	Mg-Mg	3.23			3.16		
	D-D	2.16			2.12		
M = Ca	T-D		1.75	1.70			(4×) 1.68 (2×, dis. ^a) 1.81
	T-Ca		3.14	3.14			3.13
	Ca-D		2.57	2.56			2.52
	Ca-Ca		3.63	3.62			3.56
	D-D		2.48	2.41			2.38
M = Sr	T-D		1.73	1.71			(4×) 1.69 (2×, dis.) 1.82
	T-Sr		3.28	3.31			3.30
	Sr-D		2.69	2.71			2.66
	Sr-Sr		3.79	3.82			3.76
	D-D		2.45	2.42			2.39
M = Eu	T-D			1.69			(4×) 1.70 (2×, dis.) 1.75
	T-Eu			3.28			3.27
	Eu-D			2.68			2.64
	Eu-Eu			3.78			3.73
	D-D			2.39			2.40

^aDisordered.

Ca₂IrD₅, and solid solutions (Ca,Eu)₂IrD₅, (Sr,Eu)₂IrD₅: disordered structure by npd at room temperature.⁴² *Fm* $\bar{3}$ *m*, *Z* = 4; Ir surrounded by five D atoms in a disordered average octahedral configuration similar to II; transition occurs between 200 and 275 K to partially ordered tetragonal modification *I4/mmm* similar to Sr₂IrD₅;⁴³ paramagnetic with $\mu_{\text{eff}} = 7.3\mu_{\text{B}}$; ferromagnetic below $T_{\text{C}} = 20$ K; rhodium-based ‘Mg₂RhH₅’ analog not obtained, presumably because of the formation of competing hydride Mg₂RhH_{1.1} (filled Ti₂Ni type structure) and binary Mg₂Rh (Ti₂Pd type structure).⁴⁸ Other Rh compounds known:⁴⁹ Eu₂RhH₅ and solid solutions (Sr,Eu)₂RhH₅. Interatomic distances are given in Table 3.

3.4 Na₂PtH₄ (K₂PdH₄, Na₂PdH₄)

Na₂PtH₄ by sintering NaH and Pt at about 573 K under hydrogen;⁵⁰ red-violet powder; diamagnetic from susceptibility measurements; K₂PdH₄ by heating KH with Pd at 610 K under 16 bar hydrogen pressure;⁵¹ yellow-green powder, nonmetallic; band gap of 1.2 eV predicted from theoretical band structure calculations;⁵² decomposes before melting; Na₂PdH₄ from NaH and Pd at up to 2500 bar and 770 K;⁵³ ordered structures (Figure 4) from npd on deuterides: *I4/mmm*, *Z* = 2; square-planar [PtH₄]²⁻ (or [PdH₄]²⁻) 16-electron complexes with T site symmetry *4/mmm*; surrounded by Na (K) in eightfold cubic configuration; one D site; Na₂PtH₄ transforms at about 573 K into disordered cubic

**Figure 4** Structure of Na₂PtD₄

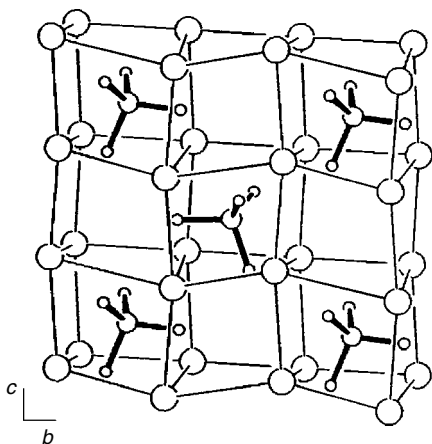
HT modification similar to II; Na₂PdH₄ does not transform up to 600 K and decomposes into Na₂PdH₂;⁵³ lif. $2\text{M}^+ \cdot [\text{TH}_4]^{2-}$; T = Pd^{II}, Pt^{II}, d⁸. Interatomic distances are given in Table 4.

3.5 Mg₂NiH₄

From binary alloy Mg₂Ni by hydrogenation at temperatures above 623 K,⁵ or by sintering powder mixtures of the elements at 723–773 K under 90 bar hydrogen pressure;³⁰ fine powder

Table 4 Interatomic distances (Å) in Na₂PtD₄ and analogs

		T = Pd	T = Pt
M = Na	T–D	1.61	1.64
	T–Na	3.14	3.12
	Na–D	2.52	2.52
	Na–Na	3.31	3.38
	D–D	2.27	2.32
M = K	T–D	1.62	
	T–K	3.49	
	K–D	2.85	
	K–K	3.84	
	D–D	2.30	

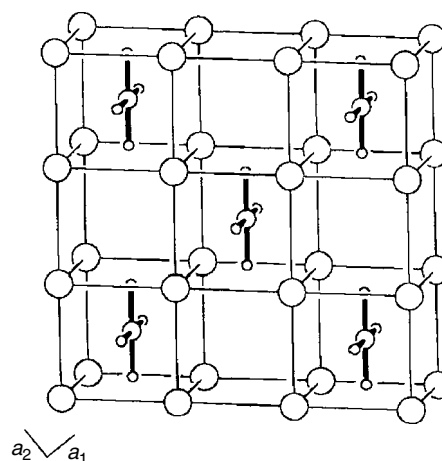
**Figure 5** Structure of Mg₂NiD₄

of dark-red (fully hydrided) or brownish (partially hydrided) color; stable in air; diamagnetic, nonmetallic; theoretical band structure calculations³⁷ on disordered structure model predict band gap of 1.8 eV; vibrational spectroscopy;⁵⁴ bonding and stability investigated by ab initio density functional calculations;^{14,55} H density: 3.6 wt%, 5.8×10^{22} H atoms cm⁻³; desorption enthalpy $\Delta H = 64$ kJ mol⁻¹ H₂; ordered structure (Figure 5) by high-resolution npd on deuteride:⁶ *C2/c*, *Z* = 8; tetrahedral [NiH₄]⁴⁻ 18-electron complex having symmetry 1; surrounded by three Mg sites in eightfold, strongly distorted cubic configuration; four D sites; X-ray and electron microscopy evidence for microtwinning⁵⁶ parallel to *bc* plane; transforms between 483 and 513 K into disordered cubic HT modification similar to II;⁵⁷ influenced by mechanical grinding;⁵⁸ lif: $2\text{Mg}^{2+} \cdot [\text{NiH}_4]^{4-}$; Ni⁰, d¹⁰.

Distances (Å) and angles: Ni–D = 1.52–1.57; D–Ni–D = 104–119°; Mg–Ni = 2.65; Ni–Ni = 4.30; Mg–Mg = 3.10; Mg–D = 1.97; D–D = 2.42.

3.6 K₂PtH₄ (Rb₂PtH₄, Cs₂PtH₄, Rb₂PdH₄, Cs₂PdH₄)

From binary hydrides and Pt(Pd) sponge at 593–693 K under 0.8 bar (Pd compounds 20 bar) hydrogen pressure;⁵⁹

**Figure 6** Structure of K₂PtD₄

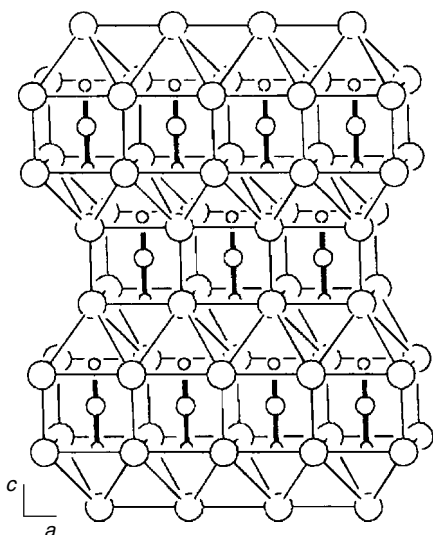
pyrophoric, colorless powders; sensitive to moisture and air; K₂PtH₄: diamagnetic; NMR data at room temperature consistent with rotational disorder of PtH₄ groups; structures from npd on deuterides at 295 and 15 K (K₂PtD₄, Rb₂PdD₄, Cs₂PdD₄), 16 K (Rb₂PtD₄), and 12 K (Cs₂PtD₄); disordered room temperature structure: cubic, *Fm* $\bar{3}$ *m*, *Z* = 4, CaF₂ type metal substructure similar to II; transforms at 250 K (Rb₂PdD₄), 225 K (Cs₂PdD₄), 195 K (K₂PtD₄), 170 K (Rb₂PtD₄), and 150 K (Cs₂PtD₄), into ordered tetragonal low-temperature (LT) structure (Figure 6): *P4*₂/*mnm*, *Z* = 2; planar [PtH₄]²⁻ (or [PdH₄]²⁻) 16-electron complexes with T site symmetry *m.mm*; unlike Na₂PtH₄, these complexes are oriented perpendicular to the tetragonal base; surrounded by M⁺ in eightfold, nearly cubic configuration; two D sites; lif: $2\text{M}^+ \cdot [\text{TH}_4]^{2-}$; T = Pd^{II}, Pt^{II}, d⁸. Interatomic distances are given in Table 5.

3.7 Na₂PdH₂ (Li₂PdH₂)

Na₂PdH₂ from NaH with Pd at 643 K under 50 bar hydrogen pressure;⁶⁰ brittle solid; single crystals show metallic luster; melts at 681 K without decomposing; metallic conductivity measured on single crystals and semiconducting behavior on powder; Li₂PdH₂⁵¹ from LiH and Pd at 680 K; melts at 773 K; electronic band structure calculations^{52,61} predict filled d bands and metallic properties in two dimensions (*ab* plane), originating from overlap between Pd d-block bands and alkali metal s- and p-block bands; Na₂PdH₂ found to be metallic;⁶¹ ordered structure of Na₂PdH₂ (Figure 7) from X-ray single-crystal diffraction on hydride and npd on deuteride: *I4/mmm*, *Z* = 2; Na₂HgO₂ type structure; linear [PdH₂]²⁻ 14-electron complexes centered on site having *4/mmm* symmetry; surrounded by Na in 10-fold bicapped cubic configuration; one D site; lif: $2\text{Na}^+ \cdot [\text{PdH}_2]^{2-}$; Pd⁰, d¹⁰; structure of Li₂PdH₂ from npd;⁵¹ evidence for linear [PtH₂]²⁻ complexes in quaternary Na₂PdH₂–Na₂PtH₄ system.⁶²

Table 5 Interatomic distances (Å) in K_2PtD_4 and analogs

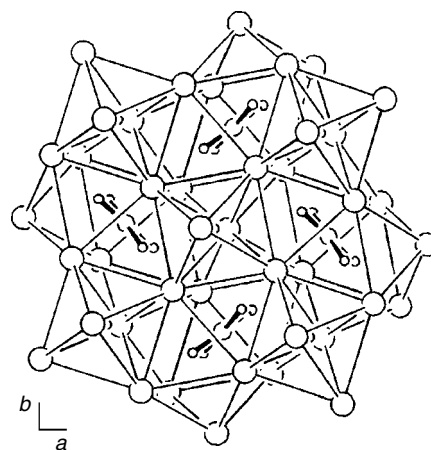
		Cubic HT-phases		Tetragonal LT-phases	
		T = Pd	T = Pt	T = Pd	T = Pt
M = K	T–D		1.62	(2×) 1.58	(2×) 1.59
	T–K		3.47		3.45
	K–D		2.86		2.83
	K–K		4.01		3.95
	D–D		2.29		2.24
M = Rb	T–D	1.63	1.63	(2×) 1.67	(2×) 1.60
				(2×) 1.67	(2×) 1.69
	T–Rb	3.64	3.63	3.61	3.60
	Rb–D	3.01	3.00	2.95	2.95
	Rb–Rb	4.21	4.19	4.12	4.14
M = Cs	D–D	2.31	2.31	2.36	2.33
	T–D	1.60	1.61	(2×) 1.59	(2×) 1.58
				(2×) 1.64	(2×) 1.61
	T–Cs	3.84	3.80	3.80	3.75
	Cs–D	3.20	3.15	3.14	3.12
	Cs–Cs	4.44	4.38	4.36	4.32
	D–D	2.26	2.28	2.28	2.25

**Figure 7** Structure of Na_2PdD_2

Distances (Å): Pd–D = (2×) 1.68 (Na), (2×) 1.67 (Li); Pd–Na(Li) = 3.13 (2.64); Pd–Pd = 3.60 (Na), 3.11 (Li); Na(Li)–D = 2.42 (2.03); D–D = 3.35 (Na), 2.85 (Li).

3.8 K_3PtH_5 (Rb_3PtH_5 , Cs_3PtH_5 , K_3PdH_5 , Rb_3PdH_5 , Cs_3PdH_5)

From binary alkali hydrides and platinum (palladium) sponge at 573–623 K under 0.8 bar (Pd compounds 70 bar) hydrogen;⁶³ colorless powders, sensitive to air and moisture; ordered structures (Figure 8) by npd on deuterides: $P4/mbm$, $Z = 2$; isostructural to Rb_3PdF_5 ; planar $[PtH_4]^{2-}$ (or

**Figure 8** Structure of K_3PtD_5

$[PdH_4]^{2-}$) 16-electron complexes with T site symmetry $m.m.m$; surrounded by two M sites in irregular ninefold configuration; two D sites, of which the twofold is octahedral surrounded by M^+ only; lif: $3M^+ \cdot [TH_4]^{2-} \cdot H^-$; T = Pd^{II} , Pt^{II} , d^8 ; K_3PtH_5 decomposes at 673 K into K_2PtH_4 and KH; Rb_3PtH_5 and Cs_3PtH_5 transform reversibly above 615 and 465 K, respectively, into disordered cubic HT modifications with Cu_3Au type metal substructure ($Pm\bar{3}m$, $Z = 1$; H positions not refined); no evidence for such transitions in Pd compounds; ordered substitution on M sites leads to quaternary hydrides K_2RbPtH_5 and K_2CsPtH_5 (H positions not refined). Interatomic distances are given in Table 6.

3.9 K_3PdH_3 (Rb_3PdH_3 , Cs_3PdH_3)

From KH and Pd sponge at 623 K under hydrogen; yellow powder at room temperature, orange-red at high temperature,⁶⁴ ordered structure (Figure 9) from npd on deuteride: $P4_2/mnm$, $Z = 8$; three Pd sites with ratios Pd1:Pd2:Pd3 = 1:1:2, each forming a linear $[PdH_2]^{2-}$ 14-electron complex having

Table 6 Interatomic distances (Å) in K_3PtD_5 and analogs

		M = K	M = Rb	M = Cs
T = Pd	Pd–D	1.63	1.61	1.64
	Pd–M	3.46	3.62	3.67
	M–D	2.84	2.99	3.04
	M–D ⁻	2.73	2.85	3.01
	M–M	3.74	4.03	4.20
	Pd–Pd	5.26	5.52	5.87
	D–D	2.20	2.17	2.30
T = Pt	Pt–D	1.63	1.58	1.64
	Pt–M	3.47	3.57	3.68
	M–D	2.74	2.98	3.03
	M–D ⁻	2.72	2.86	2.96
	M–M	3.85	4.05	4.25
	Pt–Pt	5.28	5.54	5.90
	D–D	2.23	2.14	2.25

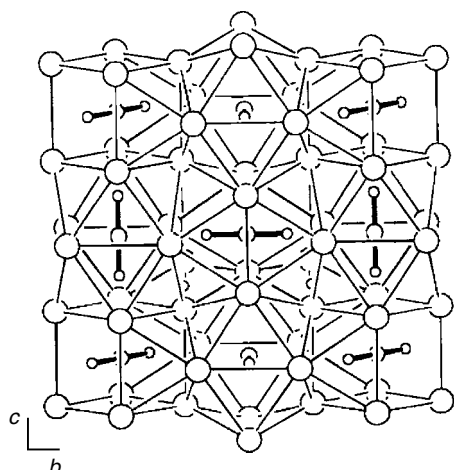


Figure 9 Structure of K_3Pd_3

respectively $m.mm$, $m.mm$, and $2/m$ environments; surrounded by three K sites in 12-fold configurations; four D sites, of which one eightfold is coordinated by K^+ in oct configuration; lif: $3K^+ \cdot [PdH_2]^{2-} \cdot H^-$; Pd^0 , d^{10} ; X-ray evidence^{59,63} for isostructural Cs_3PdH_3 and Rb_3PdH_3 ; K_3PdH_3 transforms at ~ 473 K into disordered HT modification ($Pm\bar{3}m$) with cubic Cu_3Au type metal substructure while Rb_3PdH_3 transforms into $Im\bar{3}$ HT modification.

Distances (\AA): Pd–D = $(2 \times) 1.68$ (Pd1), $(2 \times) 1.68$ (Pd2), $(2 \times) 1.69$ (Pd3); Pd–K = 3.04; K–D = 2.64, $K-D^- = 2.74$, D–D = 3.37.

3.10 $CaPdH_2$ ($SrPdH_{2.7}$, $EuPdH_3$, $YbPdH_{2.7}$, $CaNiH_3$, $YbNiH_{2.7}$)

$CaPdH_2$ from CaH_2 and Pd sponge at 1123 K under hydrogen pressures up to 300 bar;⁶⁵ disordered structure (Figure 10) from npd on deuteride at 295 and 10 K: $Pm\bar{3}m$, $Z = 1$; Pd and Ca form CsCl-type metal substructure as in binary $CaPd$; disordered D site near anion positions of perovskite-type structure with $2/3$ occupancy and large displacement amplitudes; structure model consistent with orientationally disordered linear $[PdH_2]^{2-}$ 14-electron complexes; no evidence for D ordering down to 10 K; lif: $Ca^{2+} \cdot [PdH_2]_{av}^{2-}$; Pd^0 , d^{10} ; X-ray evidence for rhombohedral distortion at room temperature;⁶⁶ copper-red $SrPdH_{2.7}$ by hydrogenation of Sr–Pd alloy;⁶⁷ structure of deuteride from npd: D site occupancy 0.91; black $EuPdH_3$ by hydrogenation of intermetallic $EuPd$ (with CrB type structure) at 15 bar hydrogen pressure at 500 K;⁶⁸ structure of deuteride from npd: full D site occupancy; metallic conductor; orders ferromagnetic at 21 K; X-ray evidence for presumably isostructural $YbPdH_{2.7}$,⁶⁹ $YbNiH_{2.7}$ ⁶⁹ and $CaNiH_3$.⁷⁰ Electronic band structure calculations on stoichiometric $APdH_3$ ($A = Sr, Eu, Yb$) predict metallic properties.⁷¹ Interatomic distances are given in Table 7.

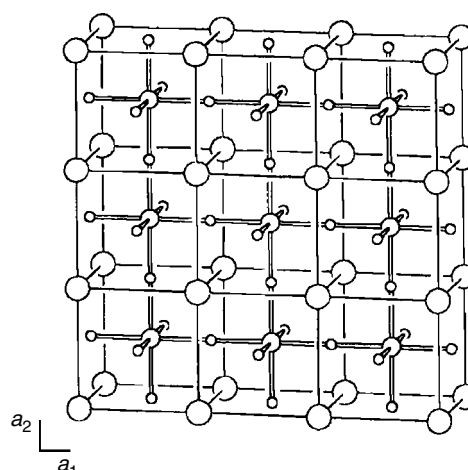


Figure 10 Structure of $CaPd_2$

Table 7 Interatomic distances (\AA) in $CaPd_2$ and analogs

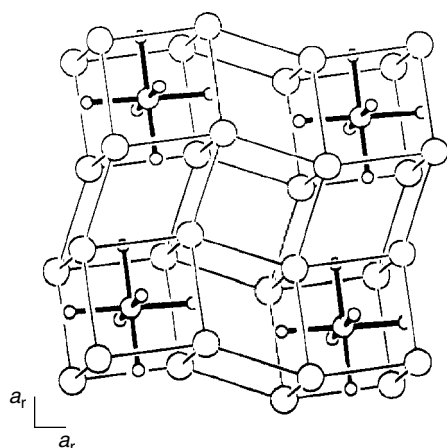
	M = Ca	M = Sr	M = Eu
Pd–D	1.84	1.92	1.90
Pd–M	3.19	3.33	3.29
M–D	2.61	2.72	2.69
M–M	3.69	3.84	3.80
D–D	2.61	2.72	2.69

3.11 Li_4RuH_6 (Na_4RuH_6 , Li_4OsH_6)

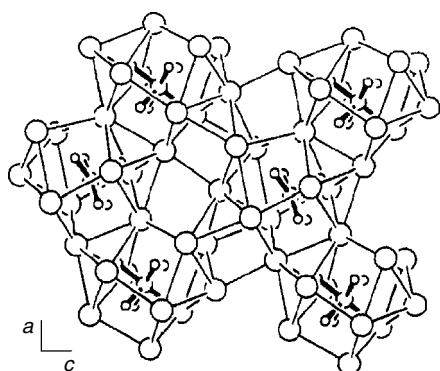
From reactions of binary hydrides MH with T at 753 K and 10 bar hydrogen pressure;⁷² no compound formation with KH and Fe up to 1073 K and 100 bar; Ru does not react with KH, and Os not with NaH and KH under experimental conditions; powders either white (Li) or green (Na); all air sensitive; ordered structures (Figure 11) from npd at room temperature on deuterides: $R\bar{3}c$, $Z = 6$ (hex setting), K_4CdCl_6 type structure; octahedral $[TH_6]^{4-}$ 18-electron complex with T site symmetry $\bar{3}$; surrounded by two M sites in nearly cubic configuration; one D site; lif: $4M^+ \cdot [TH_6]^{4-}$; T = Ru^{II} , Os^{II} , d^6 . Interatomic distances are given in Table 8.

3.12 Na_3RhH_6 (Li_3RhH_6 , Na_3IrH_6 , Li_3IrH_6)

From powder mixtures of binary MH and Ir(Rh) at 630–770 K under hydrogen;⁷³ colorless powders, sensitive to air and humidity; Li_3RhH_6 forms either during decomposition of Li_3RhH_4 ⁷⁴ in hydrogen atmosphere or by sintering powder mixtures of LiH and Rh under 80 bar hydrogen pressure at 823 K;⁷⁵ ordered structures (Figure 12) from npd on deuterides^{73,75} at 295 K (Na–Rh, Na–Ir, Li–Rh, Li–Ir) and 11 K (Na–Rh, Na–Ir); $Pnma$, $Z = 4$; isolated octahedral $[TH_6]^{3-}$ 18-electron complex with T site symmetry m ; surrounded by three M sites in irregular 11-fold coordination; four D sites; no evidence for structural phase transition in Na_3RhH_6 and

Figure 11 Structure of Li_4RuD_6 Table 8 Interatomic distances (Å) in Li_4RuD_6 and analogs

		T = Ru	T = Os
M = Li	T-D	1.71	1.71
	T-Li	2.49	2.52
	Li-D	2.05	2.13
	Li-Li	3.03	3.014
	D-D	2.41	2.27
M = Na	T-D	1.79	
	T-Na	2.84	
	Na-D	2.35	
	Na-Na	3.40	
	D-D	2.50	

Figure 12 Structure of Na_3RhD_6

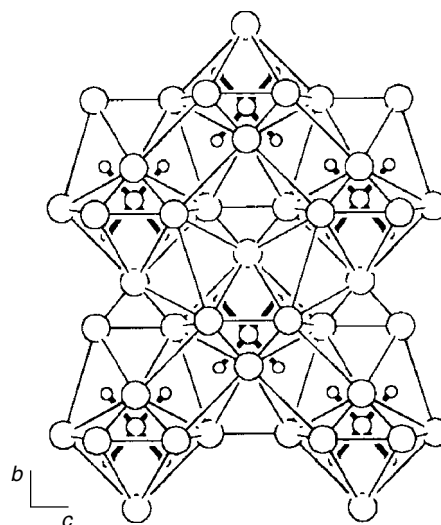
Na_3IrH_6 down to 11 K and up to 670 K; lif: $3\text{M}^+ \cdot [\text{TH}_6]^{3-}$; T = Ir^{III} , Rh^{III} ; d^6 . Interatomic distances are given in Table 9.

3.13 Li_3RhH_4

From LiH and Rh powder at 870 K under hydrogen;⁷⁴ powder of metallic appearance; oxygen and moisture sensitive;

Table 9 Interatomic distances (Å) in Na_3RhD_6 and analogs

		T = Rh	T = Ir
M = Li	T-D	1.56–1.64	1.61–1.70
	T-Li	2.66	2.72
	Li-D	1.81	1.88
	Li-Li	2.59	2.59
	D-D	2.07	2.21
M = Na	T-D	1.63–1.68	1.64–1.70
	T-Na	2.98	2.94
	Na-D	2.17	2.08
	Na-Na	3.22	3.18
	D-D	2.28	2.26

Figure 13 Structure of Li_3RhD_4

corresponds to previously reported ' Li_4RhH_5 ' as characterized by X-ray diffraction on single crystals;⁷⁶ decomposes at high temperature under 80 bar hydrogen pressure into Li_3RhH_6 (XII); ordered structure (Figure 13) by npd on deuteride: $Cmcm$; $Z = 4$; planar $[\text{RhH}_4]^{3-}$ 16-electron complexes with T site symmetry $m2m$; surrounded by two Li sites in irregular 11-fold coordination; two D sites; lif: $3\text{Li}^+ \cdot [\text{RhH}_4]^{3-}$; Rh^{I} , d^8 .

Distances (Å): Rh-D = 1.79(2×), 1.75(2×); Rh-Li = 2.31; Rh-Rh = 3.87(2×); Li-Li = 2.35; Li-D = 2.15; D-D = 2.21.

3.14 MgRhH_{1-x}

From binary alloy MgRh (CsCl-type structure) at 748 K and 130 bar hydrogen pressure;⁷⁷ powder of gray color and metallic appearance; partially disordered structure (Figure 14) by in situ npd at 39 bar, 2.5 bar and 10^{-2} mbar deuterium pressure: $P4/mmm$, $Z = 4$; one Rh and two Mg sites forming a tetragonal distorted CsCl-type structure with doubled a parameter ($2c/a = 1.012$ at 39 bar); one D site connecting

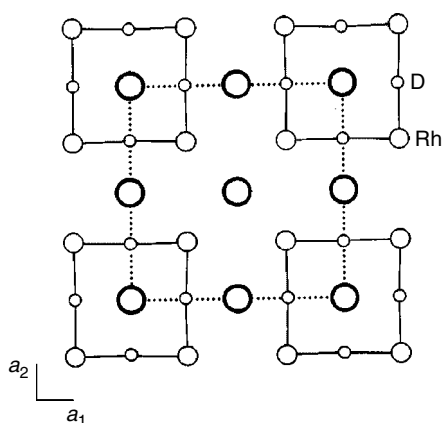


Figure 14 Structure of MgRhD_{1-x}

Rh into cyclic tetramer Rh_4D_4 having $4/mmm$ symmetry with nearly linear Rh–D–Rh and rectangular D–Rh–D bonds; occupancy of D site increasing as a function of D pressure (94% at 39 bar, 86% at 2.5 bar, 61% at 10^{-2} mbar), metal substructure resembles CaPdH_2 (X); likely phase limit near stoichiometric composition MgRhH ; lif (border case) at that composition: $4\text{Mg}^{2+} \cdot [\text{Rh}_4\text{H}_4]^{8-}$; X-ray evidence for cubic MgIrH_x phase ($a = 3.23 \text{ \AA}$) at high pressure with CsCl-type metal substructure.

Distances (\AA) at 39 bar ($\text{MgRhD}_{0.94}$): Rh–D ($2\times$) = 1.71; Mg–Rh = 2.66; Mg–D = 2.23; Rh–Rh = 2.98; Mg–Mg = 3.20; D–D = 2.36.

3.15 Mg_3RuH_3

From elements by sintering at 883 K under 9 bar hydrogen pressure;⁷⁸ dark gray powder, stable in air; partially disordered structure (Figure 15) by npd on deuteride: $P4_2/mnm$, $Z = 4$; Ru at center of orientationally disordered ts-RuH_3 units ($m.2m$ site symmetry) containing two D sites, one ordered and the other disordered (split atom position with D–D = 0.87 \AA); surrounded by two Mg sites forming an eightfold bicapped prismatic coordination; joined to dimers of $m.mmm$ site symmetry by possible Ru–Ru bond; lif: $3\text{Mg}^{2+} \cdot [\text{RuH}_3]^{6-}$ (monomer without Ru–Ru bond, 17 electrons/Ru); $6\text{Mg}^{2+} \cdot [\text{Ru}_2\text{H}_6]^{12-}$ (dimer with Ru–Ru bond, 18 electrons/Ru); Ru–Ru bond formation not supported by extended Hückel calculations.¹²

Distances (\AA): Ru–D = 1.71 (split atom), 1.71 ($2\times$); Mg–Ru = 2.73; Ru–Ru = 3.31; Mg–D = 2.01; Mg–Mg = 3.03; D–D = 0.87 (split atom), 2.52.

3.16 $\text{SrMg}_2\text{FeH}_8$ ($\text{BaMg}_2\text{FeH}_8$, $\text{EuMg}_2\text{FeH}_8$)

From binary alloys $\text{SrMg}_{2.2}$ (BaMg_2 , EuMg_2) and Fe powder at 763–783 K under 140 bar hydrogen pressure;^{66,79} green (Sr) or brownish (Ba) powder; sensitive to air; ordered structure (Figure 16) by npd on deuterides of Sr and Ba

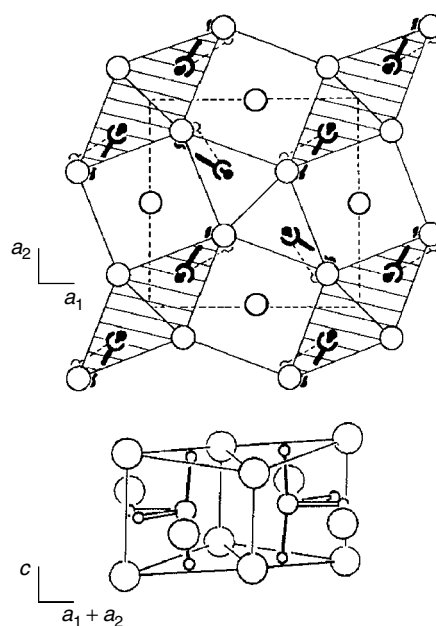


Figure 15 Structure of Mg_3RuD_3

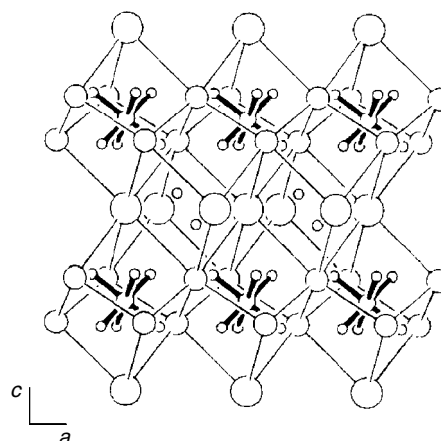


Figure 16 Structure of $\text{SrMg}_2\text{FeD}_8$

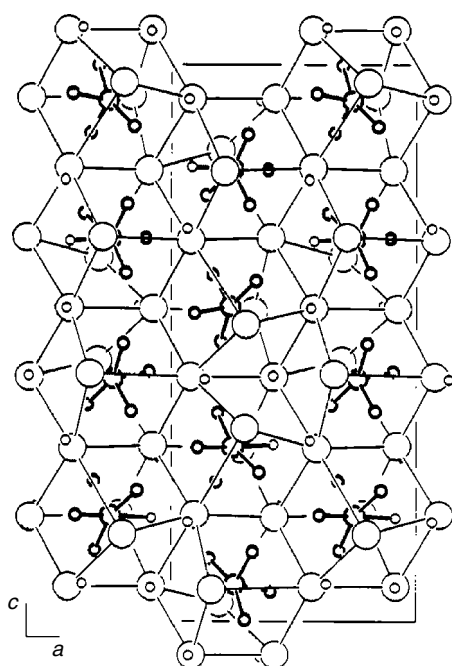
compounds: $P\bar{3}m1$, $Z = 1$; octahedral $[\text{FeH}_6]^{4-}$ 18-electron units having T site symmetry $\bar{3}m$, surrounded by eight M^{2+} in nearly cubic configuration; one Mg and one Sr(Ba) site; two D sites, of which the twofold is tetrahedrally coordinated by M^{2+} with one short Mg–D and three long Sr(Ba)–D bonds; lif: $\text{M}^{2+} \cdot 2\text{Mg}^{2+} \cdot [\text{FeH}_6]^{4-} \cdot 2\text{H}^-$; Fe^{II}, d^6 . Ru analog $\text{BaMg}_2\text{RuD}_8$ (XXXVIII) crystallizes with tetragonal symmetry. Interatomic distances are given in Table 10.

3.17 $\text{Mg}_6\text{Co}_2\text{H}_{11}$

From elements by sintering at 753–773 K under 40–50 bar hydrogen pressure;⁸⁰ black powder, stable in air; nonmetallic; pressure–composition isotherms show two plateaus of

Table 10 Interatomic distances (Å) in SrMg₂FeD₈ and barium analog

	M = Sr	M = Ba
Fe–D	1.58	1.58
Fe–Mg	2.72	2.75
Fe–M	3.28	3.46
Mg–D	2.20	2.22
Mg–D ⁻	1.92	1.92
M–D	2.65	2.81
M–D ⁻	2.66	2.74
Mg–Mg	3.06	3.08
Mg–M	3.60	3.75
D–D	2.19	2.18

**Figure 17** Structure of Mg₆Co₂D₁₁

which that at low pressure is attributed to decomposition of Mg₆Co₂H₁₁ ($\Delta H = 79 \text{ kJ mol}^{-1} \text{ H}_2$) and that at high pressure to decomposition of tetragonal Mg₂CoH₅ ($\Delta H = 79 \text{ kJ mol}^{-1} \text{ H}_2$);⁸¹ partially disordered structure (Figure 17) from joint synchrotron X-ray and high-resolution npd:⁸⁰ *Pnma*, $Z = 8$, 63 positional parameters; two eightfold Co sites, one (Co1) forming an ordered *sad*-[CoH₄]⁵⁻ 18-electron complex of symmetry 1, and the other (Co2) a partially disordered *spy* configuration with one half-occupied ligand; interpreted as a 1:1 mixture of *spy*-[CoH₅]⁴⁻ and *sad*-[CoH₄]⁵⁻ 18-electron complexes; surrounded by eight Mg sites in distorted cubic configurations; 14 D sites, of which five are surrounded by Mg in *tri* and *sad* configurations; metal substructure derives from trigonal SrMg₂FeH₈ (XVI) by orthorhombic distortion; short Mg–Mg bonds; lif: 2Mg₆Co₂H₁₁ = 12Mg²⁺·[CoH₅]_{av}⁴⁻·2[CoH₄]_{av}⁵⁻·5H⁻; mono-

clinic distorted Ir analog Mg₆Ir₂H₁₁ (XLV) has different T–H complex ordering; other hydrides with similar metal substructure: Mg₃RuH₆ (XXV), Mg₃ReH₇ (XXIII), and LiMg₂RuH₇ (XXVII).

Distances (Å): Co1–D = 1.52–1.57, Co2–D = 1.51–1.62; Co–Co = 4.58; Co–Mg = 2.52; Mg–Mg = 2.78; Mg–D = 1.94; Mg–D⁻ = 1.82; D–D = 2.09.

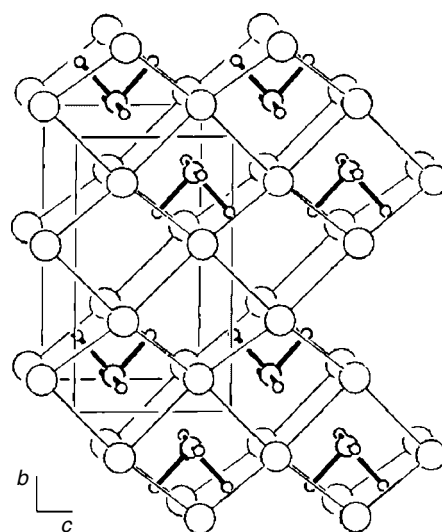
3.18 Mg₂RuH₄

From the elements, by sintering at 723 K under 20 bar, or at 1050 K under 160 bar hydrogen pressure;⁸² powder of reddish-brown to dark-red color, sensitive to moisture and air; ordered structure (Figure 18) from npd on deuteride: *Cmcm*, $Z = 4$; *sad*-[RuH₄]⁴⁻ 16-electron complex with T site symmetry *m2m*, derives from the oct-[RuH₆]⁴⁻ complex in Mg₂RuH₆ by removal of two *cis* D ligands; two D sites; surrounded by Mg in eightfold distorted cubic configuration, neighboring cubes share faces; possible Ru–Ru interactions across these faces (Ru–Ru = 3.24 Å) could lead to polyanionic [RuH₄]_n⁴ⁿ⁻ zig-zag chains running along *c*; magnetic measurements consistent with d⁸ low-spin configuration; lif: 2Mg²⁺·[RuH₄]⁴⁻ (monomer); Ru⁰, d⁸; 2nMg²⁺·[Ru_nH_{4n}]⁴ⁿ⁻ (polymer); Ru–Ru bonds not supported by extended Hückel calculations.¹²

Distances (Å) and angles: Ru–D = 1.67(2×), 1.68(2×); D–Ru–D = 84.2°, 93.6° (*cis*), 170.3° (*trans*); Ru–Mg = 2.69; Ru–Ru = 3.24(2×); Mg–D = 2.10; Mg–Mg = 2.93; D–D = 2.23.

3.19 CaMgNiH₄ (SrMgNiH₄, YbMgNiH₄, EuMgNiH₄)

From mixtures of arc-melted binary alloys (CaNi₂, CaMg₂, SrNi, YbNi, EuNi) or Mg sintered at 723–763 K under

**Figure 18** Structure of Mg₂RuD₄

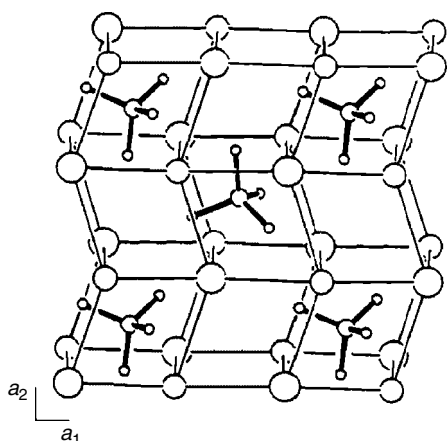


Figure 19 Structure of CaMgNiD_4

Table 11 Interatomic distances (Å) in CaMgNiD_4 and analogs

	M = Ca	M = Sr	M = Yb
Ni–D	1.59–1.61	1.54–1.64	1.57–1.62
Ni–Mg	2.54	2.55	2.53
Ni–M	3.03	3.21	3.03
Mg–D	2.08	2.15	2.09
M–D	2.45	2.53	2.43
Mg–Mg	4.18	4.24	4.15
Mg–M	3.48	3.54	3.50
D–D	2.59	2.54	2.60
D–Ni–D	108°, 111°	108°, 111°	109°, 110°

130–140 bar hydrogen pressure;⁸³ greenish (Ca, Sr) or black (Yb) powders; translucent single crystals of CaMgNiH_4 having yellow–brownish color obtained by sintering binary hydrides with LiH flux in Ni crucible at 737 K under 95 bar hydrogen pressure;⁸⁴ desorption enthalpy $\Delta H = 129(3)$ (Ca), 111(3) (Yb) $\text{kJ mol}^{-1} \text{H}_2$; ordered structures (Figure 19) from npd on deuterides (Ca, Sr, and Yb⁸³): $P2_13$, $Z = 4$; tetrahedral $[\text{NiH}_4]^{4-}$ 18-electron complex having T site symmetry 3, surrounded by one Ca (Sr, Yb) site, and one Mg site in ordered distorted cubic configuration; two D sites; derived from Mg_2NiD_4 (V) by partial substitution of Mg; lif: $\text{M}^{2+} \cdot \text{Mg}^{2+} \cdot [\text{NiH}_4]^{4-}$; Ni^0 , d^{10} ; X-ray evidence for isostructural EuMgNiH_4 .⁸³ Interatomic distances are given in Table 11.

3.20 $\text{Ca}_4\text{Mg}_4\text{Fe}_3\text{H}_{22}$ ($\text{Yb}_4\text{Mg}_4\text{Fe}_3\text{H}_{22}$)

From mixtures of arc-melted binary alloys (CaMg, YbMg) and Fe powder, by adding LiH as a flux, at about 773–793 K under 100–150 bar hydrogen pressure;⁸⁵ $\text{Ca}_4\text{Mg}_4\text{Fe}_3\text{H}_{22}$: brownish powder containing brownish translucent single crystals; $\text{Yb}_4\text{Mg}_4\text{Fe}_3\text{H}_{22}$: black powder; both stable in air for several weeks; desorption enthalpies $\Delta H = 122(4)$ (Ca), 137(3) (Yb) $\text{kJ mol}^{-1} \text{H}_2$; decomposition of Ca compound

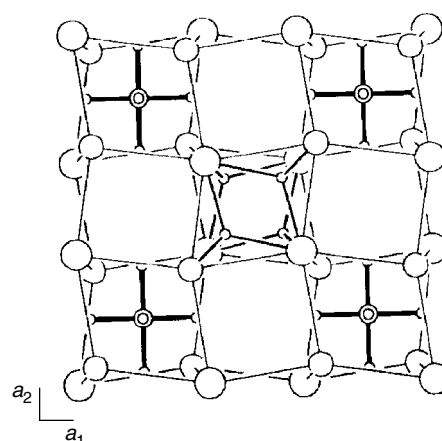


Figure 20 Structure of $\text{Ca}_4\text{Mg}_4\text{Fe}_3\text{D}_{22}$

Table 12 Interatomic distances (Å) in $\text{Ca}_4\text{Mg}_4\text{Fe}_3\text{D}_{22}$ and ytterbium analog

	M = Ca	M = Yb
Fe–D	1.56–1.58	1.55–1.59
Fe–Mg	2.79	2.78
Fe–M	3.09	3.06
Mg–D	2.07	2.02
Mg–D ⁻	1.81	1.91
M–D	2.43	2.41
M–D ⁻	2.39	2.41
Mg–Mg	4.08	3.98
Mg–M	3.39	3.40
D–D	2.22	2.22

shows two plateaus: formation of Ca_2FeH_6 , Mg, Fe, and H_2 (upper plateau), and of CaH_2 , Fe, and H_2 (lower plateau); decomposition of Yb compound shows one plateau: formation of YbH_2 , Mg, Fe, and H_2 ; ordered structures (Figure 20) from single-crystal X-ray ($\text{Ca}_4\text{Mg}_4\text{Fe}_3\text{H}_{22}$) and npd on deuterides; $P43m$, $Z = 1$; octahedral $[\text{FeH}_6]^{4-}$ 18-electron complexes with T site symmetry $\bar{4}2.m$, surrounded by one M and one Mg site in deformed cubic configuration; three D sites, of which the fourfold is tetrahedrally surrounded by one Mg^{2+} and three M^{2+} ; derived from Mg_2FeH_6 (II) by partial substitution of Mg by Ca, and of every fourth $[\text{FeH}_6]^{4-}$ by 4H^- ; lif: $4\text{M}^{2+} \cdot 4\text{Mg}^{2+} \cdot 3[\text{FeH}_6]^{4-} \cdot 4\text{H}^-$; Fe^{II} , d^6 . Interatomic distances are given in Table 12.

3.21 Ba_2PtH_6 (Sr_2PtH_6)

From BaH_2 (SrH_2) and Pt powder in hydrogen;⁸⁶ ordered Ba_2CuF_6 type structure (Figure 21) from npd on deuteride: $Cmca$, $Z = 4$; planar $[\text{PtD}_4]^{2-}$ 16-electron complexes with T site symmetry $2/m$, surrounded by M in 10-fold bicapped cubic configuration; three D sites, of which one eightfold is tetrahedrally surrounded by M^{2+} ; lif: $2\text{M}^{2+} \cdot [\text{PtH}_4]^{2-} \cdot 2\text{H}^-$; Pt^{II} , d^8 .

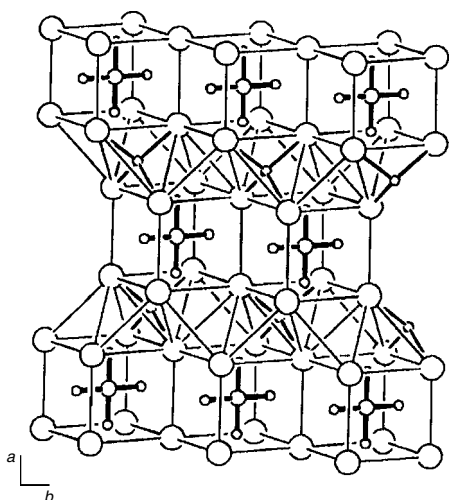


Figure 21 Structure of Ba_2PtD_6

Distances (Å): Pt–D = 1.66(2×) and 1.67 (2×); Pt–Ba = 3.63; Pt–Pt = 4.24; Ba–Ba = 4.09; Ba–D = 2.97; Ba–D[−] = 2.62; D–D = 2.36.

3.22 $\text{LiSr}_2\text{PdH}_5$

From reaction of arc-melted ternary alloy $\text{Li}_{1.5}\text{Sr}_2\text{Pd}$ at 793–803 K under 155 bar hydrogen pressure;⁸⁷ dark-green powder, sensitive to air; partially disordered structure (Figure 22) from npd on deuteride at 14 K: $P4/mmm$, $Z = 1$; metals form ordered superstructure of CsCl; contains ordered SrLiD_3 type slabs having inverse perovskite-type structure; Pd surrounded by three D, on average, in partially disordered octahedral configuration with four half occupied equatorial D sites forming linear Pd–D–Pd bridges similar to those in CaPdH_2 (X), and two fully occupied axial sites belonging to the SrLiD_3 type slabs; both have large displacement amplitudes; three D sites, of which a twofold is octahedral surrounded

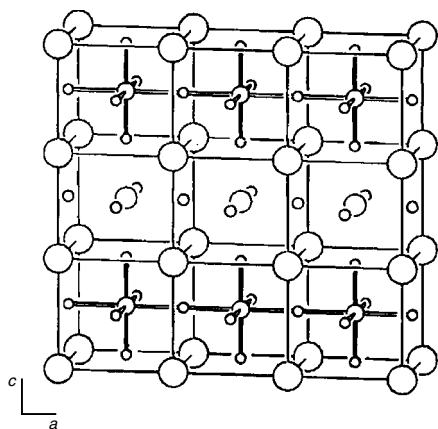


Figure 22 Structure of $\text{LiSr}_2\text{PdD}_5$

by four Sr and two Li; lif: $\text{Li}^+ \cdot 2\text{Sr}^{2+} \cdot [\text{PdH}_3]_{\text{av}}^{3-} \cdot 2\text{H}^-$; Pd^0 , d^{10} (average).

Distances (Å): Pd–D = 1.69(2×), 1.95 (4×, disordered); Pd–Sr = 3.34; Pd–Li = 3.70; Pd–Pd = 3.90; Li–D = 2.01; Li–D[−] = 1.95; Li–Sr = 3.30; Sr–D = 2.71; Sr–D[−] = 2.66; D–D = 2.58.

3.23 Mg_3ReH_7 (Mg_3MnH_7)

From elements by sintering powder mixtures at 783–793 K under 120 bar hydrogen pressure;⁸⁸ gray powder; sensitive to air; orange-red Mn analog Mg_3MnH_7 from powder mixtures of MgH_2 and Mn at 20 kbar pressure and 1073 K in multianvil device;⁸⁹ ordered structures (Figure 23) by npd on deuterides: $P6_3/mmc$, $Z = 2$; octahedral $[\text{TH}_6]^{5-}$ 18-electron complexes with T site symmetry $\bar{3}m$, surrounded by two Mg sites in eightfold distorted cubic configuration similar to that of $\text{SrMg}_2\text{FeH}_8$ (XVI); two D sites, of which the twofold is surrounded by Mg in trigonal bipyramidal configuration with two short collinear and three long triangular Mg–D bonds; lif: $3\text{Mg}^{2+} \cdot [\text{TH}_6]^{5-} \cdot \text{H}^-$; T^I, d^6 ; electronic band structure calculation on Mn compound.⁹⁰ Interatomic distances are given in Table 13.

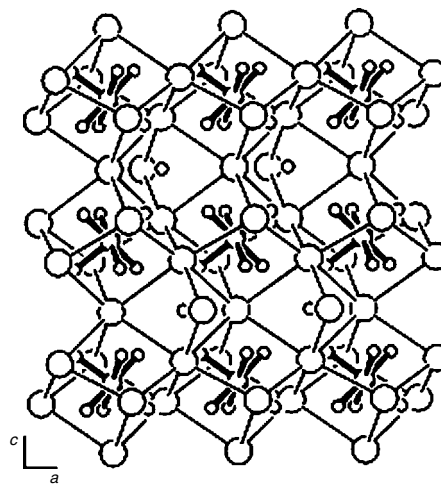


Figure 23 Structure of Mg_3ReD_7

Table 13 Interatomic distances (Å) in Mg_3ReD_7 and manganese analog

	T = Mn	T = Re
T–D	1.63	1.72
T–Mg	2.56	2.64
T–T	4.70	4.85
Mg–D	2.08	2.14
Mg–D [−]	1.87	1.90
Mg–Mg	3.05	3.17
D–D	2.29	2.41

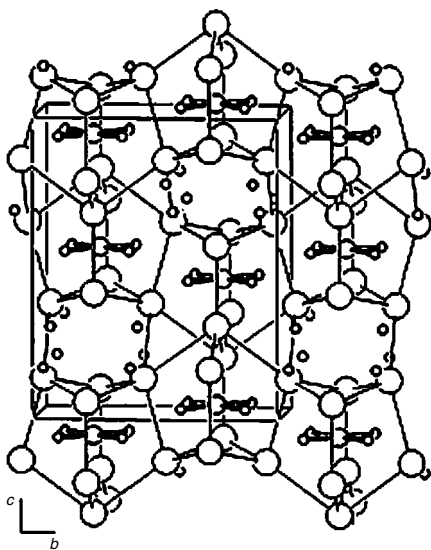


Figure 24 Structure of Mg_4IrD_5

3.24 Mg_4IrH_5

From elements by sintering powder mixtures at 783 K and 41 bar hydrogen pressure;⁹¹ dark gray powder, stable in air; presumably metallic; partially disordered structure (Figure 24) from npd on deuteride at room temperature and 9 K: $Imma$, $Z = 4$; Ir surrounded by three D atoms, on the average, in disordered planar configuration with 75% occupancy (average T site symmetry $mm2$); surrounded by three Mg sites in irregular ninefold coordination; two D sites, of which the eightfold is coordinated by Mg in saddle-like configuration; short Mg–Mg bonds along backbone of $[\text{Mg}_9\text{IrD}_3]$ units; no apparent homogeneity range; lif (border case): $4\text{Mg}^{2+} \cdot [\text{IrH}_3]_{\text{av}}^{6-} \cdot 2\text{H}^-$.

Distances (Å): Ir–D = 1.70(4×, dis); Ir–Mg = 2.75; Ir–Ir = 4.62; Mg–Mg = 2.76; Mg–D = 2.15; Mg–D[−] = 1.88; D–D = 2.34.

3.25 Mg_3RuH_6

From elements by sintering powder mixtures at 1053 K under 90 bar hydrogen pressure;⁹² powder of rusty-brown color, sensitive to moisture and air; partially disordered structure (Figure 25) from npd on deuteride at room temperature and 15 K: $Cmcm$, $Z = 4$; Ru surrounded by five D, on average, in disordered octahedral configuration (average T site symmetry $2/m$); equatorial sites have 75% and axial sites full occupancy; surrounded by two Mg sites in eightfold cubic configuration similar to Mg_3ReH_7 (XXIII); three D sites, of which the fourfold is coordinated by two Mg in linear configuration; no indication for D ordering down to 15 K; lif: $3\text{Mg}^{2+} \cdot [\text{RuH}_5]_{\text{av}}^{5-} \cdot \text{H}^-$; Ru^0 , d^8 (average).

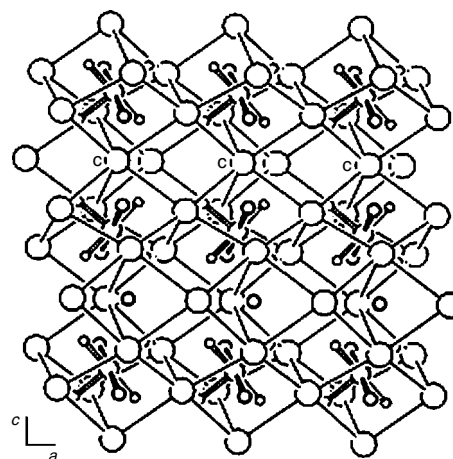


Figure 25 Structure of Mg_3RuD_6

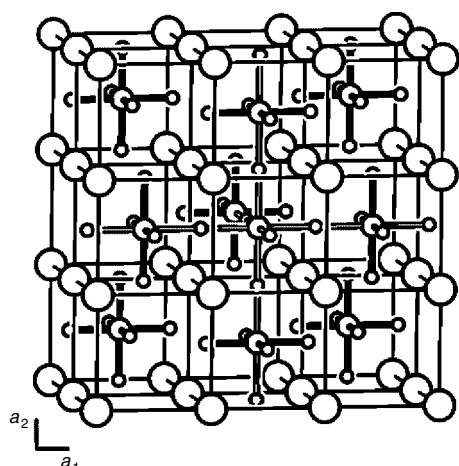
Distances (Å): Ru–D = 1.66 (4×, dis), 1.73 (2×); Ru–Mg = 2.67; Ru–Ru = 4.79; Mg–Mg = 3.04; Mg–D = 1.91; Mg–D[−] = 1.87; D–D = 2.29.

3.26 $\text{Sr}_8\text{Rh}_5\text{H}_{23}$ ($\text{Ca}_8\text{Rh}_5\text{H}_{23}$)

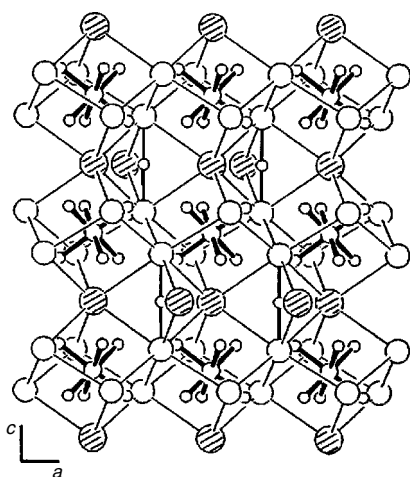
From alkaline earth hydrides and rhodium metal by sintering powder mixtures at 1073 K under 5 bar hydrogen pressure;^{46,47,93} powder of black-red (Sr) and black (Ca) color, sensitive to moisture and air; partially disordered, structure intermediate to anion deficient K_2PtCl_6 type (II) and perovskite type (Figure 26); from npd on deuterides (Sr, Ca)^{46,93} at room temperature and 10 K: $Pm\bar{3}m$, $Z = 1$; three D sites of which two are terminal to Rh with full occupancies and one sixfold is bridging two Rh with partial occupancy (5/6); 3 Rh sites surrounded in octahedral configurations (site symmetries $m\bar{3}m$ and $4/m\bar{m}m$) by six ordered terminal (Rh1), six disordered (5/6 occupancy) bridging (Rh3), and four ordered terminal plus two disordered bridging (Rh2) deuterium sites, the two latter forming a quasi-infinite polynuclear $[\text{Rh}_4\text{H}_{17}]_n^{13n-}$ complex; one Sr (Ca) site surrounds Rh in eightfold cubic configuration; no indication for D ordering down to 10 K; lif: $8n\text{M}^{2+} \cdot n[\text{RhH}_6]^{3-} \cdot [\text{Rh}_4\text{H}_{17}]_n^{13n-}$ mixed valence Rh^{I} (d^8) and Rh^{III} (d^6). Interatomic distances are given in Table 14.

3.27 $\text{LiMg}_2\text{RuH}_7$ ($\text{LiMg}_2\text{OsH}_7$)

From LiH, Mg, and Ru (Os) powders at up to 823 K under hydrogen pressure of up to 155 bar;^{94,95} light yellow powder; sensitive to air; ordered derivative of Mg_3ReH_7 type (XXIII) structure (Figure 27) by npd on deuteride of Ru compound: $P6_3/mmc$, $Z = 2$; octahedral $[\text{RuH}_6]^{4-}$ 18-electron units having T site symmetry $\bar{3}m$, surrounded by six Mg^{2+} and two Li^+ in nearly cubic configuration; one Mg and one Li site; two D sites, of which the twofold is trigonal

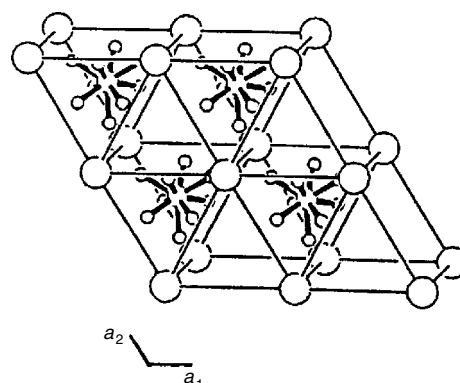
Figure 26 Structure of $\text{Sr}_8\text{Rh}_5\text{D}_{23}$ Table 14 Interatomic distances (Å) in $\text{Sr}_8\text{Rh}_5\text{D}_{23}$ and calcium analog

	M = Ca	M = Sr
Rh1–D	1.69(6×)	1.69(6×)
Rh2–D	1.70(4×)	1.70(4×)
	1.77(2×, dis)	1.89(2×, dis)
Rh3–D	1.87(6×, dis)	1.92(6×, dis)
Rh–M	3.14	3.29
Rh–Rh	3.64	3.81
M–D	2.56	2.69
M–M	3.62	3.80
D–D	2.39	2.38

Figure 27 Structure of $\text{LiMg}_2\text{RuD}_7$

bipyramidal coordinated with two short linear Mg–D and three long triangular Li–D bonds; lif: $\text{Li}^+ \cdot 2\text{Mg}^{2+} \cdot [\text{RuH}_6]^{4-} \cdot \text{H}^-$; $\text{Ru}^{\text{II}}, d^6$.

Distances (Å): Ru–D = 1.69(6×); Ru–Mg = 2.83; Ru–Li = 2.67; Ru–Ru = 4.70; Mg–Li = 3.29; Mg–Mg =

Figure 28 Structure of BaReH_9

3.17; Li–D = 2.14; Li–D[−] = 2.71; Mg–D = 2.27; Mg–D[−] = 1.85; D–D = 2.34.

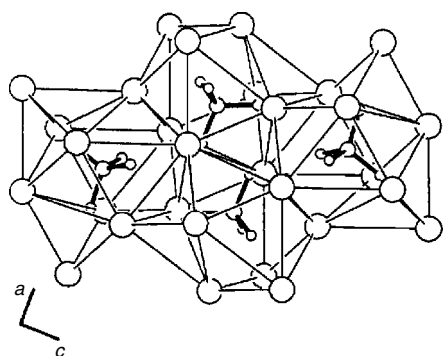
3.28 BaReH_9

From di-sodium salt Na_2ReH_9 (obtained from reaction of KReO_4 with K metal in ethylene diamine–water solution) converted to the di-potassium salt by way of the Ba salt;⁹⁶ white powder, transparent crystals, unstable in moist air; ordered structure (Figure 28) from single-crystal X-ray diffraction, and IR and NMR data on hydride:⁹⁷ $P6_3/mmc$, $Z = 2$; Re site forming $\text{ttp}[\text{ReH}_9]^{2-}$ 18-electron complexes with site symmetry $6m2$; surrounded by Ba cations in NiAs type configuration; two H sites (not refined); lif: $\text{Ba}^{2+} \cdot [\text{ReH}_9]^{2-}$; $\text{Re}^{\text{VII}}, d^0$; electronic band structure by APW calculations.⁹⁸

Interatomic distances (Å): Re–H ~ 1.69^a (3× and 6×); Re–Ba = 3.84; Re–Re = 5.29; Ba–Ba = 4.66; Ba–H = 2.71^a, 2.86; H–H ~ 1.97^a (distances not refined).

3.29 K_2ZnH_4 (Rb_2ZnH_4 , Cs_2ZnH_4 , Sr_2PdH_4 , Ba_2PdH_4 , Eu_2PdH_4)

M_2ZnH_4 (M = K, Rb, Cs) from elements by sintering powder mixtures at 783–793 K under 120 bar hydrogen pressure;^{99,100} M_2PdH_4 (M = Sr, Ba,¹⁰¹ Eu¹⁰²), from elements gray powder; sensitive to air; ordered structure (Figure 29) by npd on deuteride: $Pnma$, $Z = 2$; $\beta\text{-K}_2\text{SO}_4$ type structure, tetrahedral $[\text{ZnH}_4]^{2-}$ 18-electron complexes with T site symmetry m surrounded by two M sites in eightfold distorted square antiprismatic configuration; three D sites; evidence for nonconducting behavior of Sr_2PdH_4 and Ba_2PdH_4 (measurement on powdered hydrides);¹⁰¹ electronic band structure on Eu_2PdH_4 ;¹⁰³ lif: $2\text{K}^+ \cdot [\text{ZnH}_4]^{2-}$; $\text{Zn}^{\text{II}}, d^{10}$; $2\text{M}^{2+} \cdot [\text{TH}_4]^{4-}$, Pd^0, d^{10} . Interatomic distances are given in Table 15.

Figure 29 Structure of K_2ZnD_4 Table 15 Interatomic distances (Å) in K_2ZnD_4 and analogs

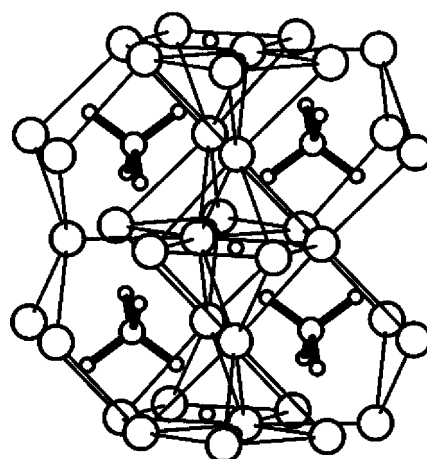
		M = K	M = Rb	M = Cs	
T = Zn	Zn–D	1.63–1.66	1.66–1.68	1.67–1.69	
	Zn–M	3.31	3.49	3.59	
	M–D	2.72	2.89	2.97	
	Zn–Zn	4.97	5.24	5.56	
	M–M	3.86	3.94	4.12	
	D–D	2.69	2.72	2.73	
T = Pd			M = Sr	M = Ba	M = Eu
	Pd–D	1.76–1.81	1.78–1.81	1.67–1.83	
	Pd–M	3.09	3.23	3.07	
	M–D	2.49	2.72	2.54	
	Pd–Pd	4.83	5.07	4.78	
	M–M	3.65	3.78	3.57	
D–D	2.58	2.80	2.69		

3.30 K_3ZnH_5 (Rb_3ZnH_5 , Cs_3ZnH_5 , Cs_3CdH_5 , K_3MnH_5 , Rb_3MnH_5 , Cs_3MnH_5)

M_3ZnH_5 (M = K, Rb, Cs) from elements by sintering powder mixtures at 783–793 K under 120 bar hydrogen pressure;^{104,105} M_3MnH_5 (M = Sr, Ba) from alkali metal hydrides and Mn powder at 875 K and 3 kbar H_2 gas pressure;^{106,107} Cs_3CdH_5 ¹⁰⁸ from elements, gray (Zn, Cd) and rose colored (Mn) powders; sensitive to air; ordered structure (Figure 30) by npd on deuteride: $I4/mcm$, $Z = 4$; Cs_3CoCl_5 type structure, tetrahedral $[TH_4]^{2-}$ 18-electron complexes with T site symmetry $\bar{4}2m$ surrounded by two M sites in an eightfold configuration; two D sites, of which the fourfold is surrounded by M in octahedral configuration; arrangement of H^- and $[TH_4]^{2-}$ complexes similar to that in K_3PtH_5 (VIII); vibrational spectroscopy of Rb_3ZnH_5 ;⁵⁴ lif: $3M^+ \cdot [TH_4]^{2-} \cdot H^-$; Zn^{II} , d^{10} ; Cd^{II} , d^{10} ; Mn^{II} , d^5 ; Mn compounds order magnetically below 50 K.⁹ Interatomic distances are given in Table 16.

3.31 $Ba_3Ir_2H_{12}$

From powder mixtures of BaH_2 and Ir at 837 K and 80 bar hydrogen pressure;¹⁰⁹ white powder, sensitive to air;

Figure 30 Structure of K_3ZnD_5 Table 16 Interatomic distances (Å) in K_3ZnD_5 and analogs

		M = K	M = Rb	M = Cs
T = Zn	Zn–D	1.66	1.66	1.68
	Zn–M	3.41	3.56	3.72
	M–D	2.75	2.94	3.15
	M–D ⁻	2.78	2.91	3.04
	Zn–Zn	5.36	5.61	5.87
	M–M	3.92	4.10	4.26
T = Cd	D–D	2.66	2.69	2.72
	Cd–D			1.82
	Cd–M			3.83
	M–D			3.11
	M–D ⁻			3.08
	Cd–Cd			5.96
T = Mn	M–M			4.35
	D–D			2.93
	Mn–D	1.75	1.76	1.79
	Mn–M	3.55	3.69	3.82
	M–D	2.73	2.88	3.11
	M–D ⁻	2.80	2.92	3.07
	Mn–Mn	5.43	5.66	5.94
	M–M	3.96	4.12	4.34
	D–D	2.78	2.85	2.87

ordered structure (Figure 31) from npd on deuteride at room temperature; $P\bar{3}m1$, $Z = 1$; octahedral $[IrH_6]^{3-}$ 18-electron complex with Ir site symmetry $3m$; surrounded by two Ba sites in irregular sevenfold coordination; two D sites; lif: $3Ba^{2+} \cdot 2[IrH_6]^{3-}$, Ir^{III} , d^6 .

Distances (Å): Ir–D = 1.60(3×) and 1.76(3×); Ir–Ba = 3.30; Ir–Ir = 5.43; Ba–D = 2.72; D–D = 2.25.

3.32 $Ca_4Mg_4Co_3H_{19}$ ($Yb_4Mg_4Co_3H_{19}$)

From mixtures of arc-melted binary alloys (CaMg, YbMg) and Co rods, by adding LiH as a flux, at up to 800 K and 155 bar hydrogen pressure;¹¹⁰ black powders, Ca compound containing brownish translucent single crystals; partially

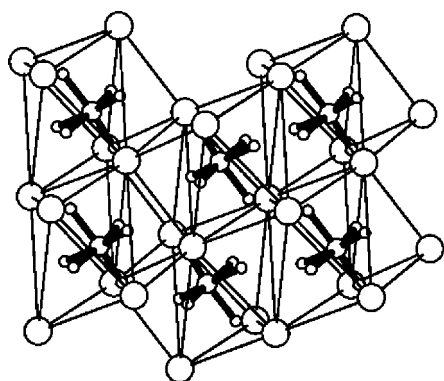


Figure 31 Structure of $\text{Ba}_3\text{Ir}_2\text{D}_{12}$

Table 17 Interatomic distances (Å) in $\text{Ca}_4\text{Mg}_4\text{Co}_3\text{D}_{19}$ and ytterbium analog

	M = Ca	M = Yb
Co-D	1.55–1.59	1.55–1.58
Co-Mg	2.75	2.74
Co-M	3.11	3.10
Mg-D	1.91	1.89
Mg-D ⁻	1.96	1.94
M-D	2.44	2.43
M-D ⁻	2.35	2.36
Co-Co	4.72	4.71
Mg-Mg	3.72	3.67
Mg-M	3.42	3.40
D-D	2.19	2.19

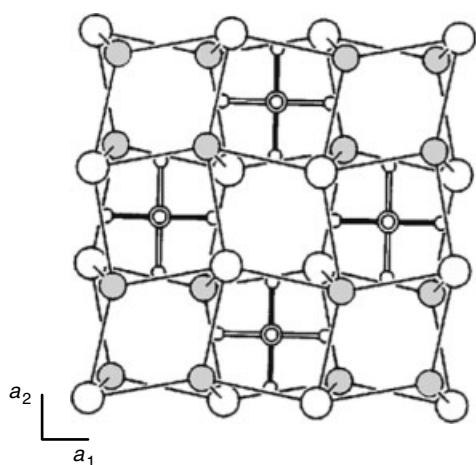


Figure 32 Structure of $\text{Ca}_4\text{Mg}_4\text{Co}_3\text{D}_{19}$

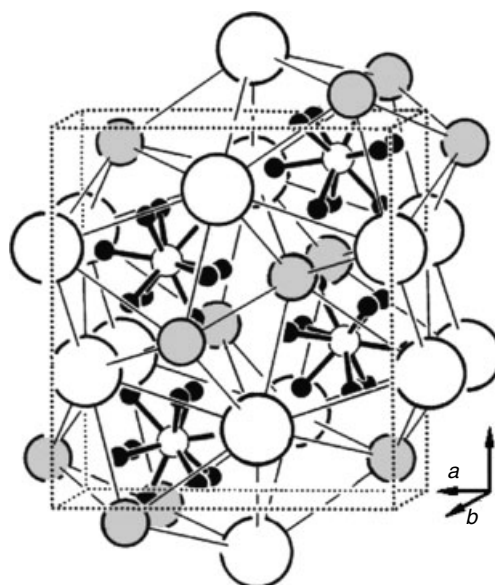


Figure 33 Structure of KNaReH_9

disordered structures (Figure 32) from npd on deuterides and single-crystal X ray on $\text{Ca}_4\text{Mg}_4\text{Co}_3\text{H}_{19}$; $P\bar{4}3m$, $Z = 1$; derives from Fe analog $\text{Ca}_4\text{Mg}_4\text{Fe}_3\text{H}_{22}$ (XX) by substitution of oct $[\text{FeH}_6]^{4-}$ by spy $[\text{CoH}_5]^{4-}$ 18-electron complexes; apical Co ligands disordered (half occupancy), Co site symmetry $\bar{4}2.m$, surrounded by Mg and Ca (Yb) sites in deformed cubic configuration; three D sites, of which one anionic D⁻ tetrahedral surrounded by one Mg^{2+} and three M^{2+} ; derives from Mg_2CoH_5 (III) by partial substitution of Mg by Ca, and of every fourth $[\text{CoH}_5]^{4-}$ by 4H^- ; lif: $4\text{M}^{2+} \cdot 4\text{Mg}^{2+} \cdot 3[\text{CoH}_5]_{\text{av}}^{4-} \cdot 4\text{H}^-$; Co^I , d^8 . Interatomic distances are given in Table 17.

3.33 KNaReH_9

Translucent crystals obtained from di-sodium salt Na_2ReH_9 ⁹⁶ by slow evaporation of a solution in KOH; unstable in moist air; ordered structure (Figure 33) from single-crystal X-ray diffraction at 193 K, and IR data:¹¹¹ $Pnma$, $Z = 4$; Re site forming ttp- $[\text{ReH}_9]^{2-}$ 18-electron complexes with site symmetry m ; surrounded by K and Na cations in

TiNiSi type metal configuration; six H sites (not refined); lif: $\text{K}^+ \cdot \text{Na}^+ \cdot [\text{ReH}_9]^{2-}$; Re^{VII} , d^0 .

Interatomic distances (Å): Re-H = 1.69–1.71^a; Re-Na = 3.35; Re-K = 3.69; Re-Re = 5.33; Na-Na = 4.00; Na-K = 4.01; K-K = 4.49; Na-H = 2.33^a; K-H = 2.61^a; H-H = 1.73^a (not refined).

3.34 $\text{Li}_5\text{Pt}_2\text{H}_9$

From reaction of LiH and Pt at 1250 bar H_2 pressure and 820 K;¹¹² anthracite colored caked solid, sensitive to air and moisture; ordered structure (Figure 34) from npd on deuteride: $I4/mcm$, $Z = 4$; contains $[\text{Pt}_2\text{H}_9]^{5-}$ dimer with $m.m$ symmetry in which four D surround each Pt in spl configuration and one D bridges two Pt; 2 Li sites; diamagnetic; lif: $5\text{M}^+ \cdot [\text{T}_2\text{H}_9]^{5-}$; Pt^{II} , d^8 .

Distances (Å): Pt-D = 1.64(4 \times), 1.85; Pt - Li = 2.64; Pt-Pt = 3.71; Li-D = 2.13; D-D = 2.28.

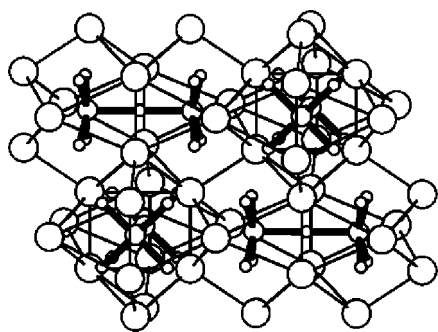


Figure 34 Structure of $\text{Li}_5\text{Pt}_2\text{D}_9$

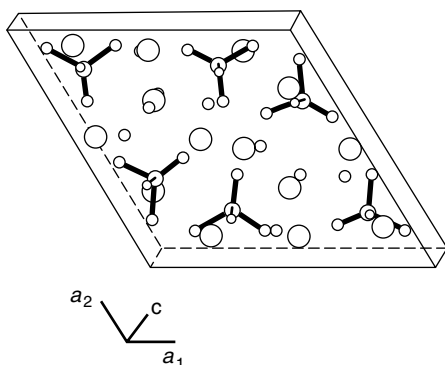


Figure 35 Structure of $\text{Ba}_7\text{Cu}_3\text{D}_{17}$

3.35 $\text{Ba}_7\text{Cu}_3\text{H}_{17}$

By hydrogenation of Ba–Cu alloys at 10 bar H_2 pressure and room temperature, followed by annealing at 643 K under 160 bar H_2 pressure;¹¹³ dark brownish powder sensitive to air and moisture; ordered structure (Figure 35) from npd on deuteride: $P31c$, $Z = 2$; contains distorted 18-electron tetrahedral $[\text{CuD}_4]^{3-}$ complexes (symmetry 1) surrounded by nine Ba (three sites) in ttp configuration; seven D sites, of which three anionic D^- tetrahedral surrounded by four M^{2+} ; lif: $7\text{Ba}^{2+} \cdot 3[\text{CuH}_4]^{3-} \cdot 5\text{H}^-$; Cu^{I} , d^{10} .

Distances (\AA): $\text{Cu}-\text{D} = 1.64\text{--}1.75$; $\text{Cu}-\text{Ba} = 3.19$; $\text{Cu}-\text{Cu} = 5.07$; $\text{Ba}-\text{D} = 2.36$; $\text{Ba}-\text{D}^- = 2.59$; $\text{D}-\text{D} = 1.94$.

3.36 $\text{LiMg}_4\text{Os}_2\text{H}_{13}$ ($\text{LiMg}_4\text{Ru}_2\text{H}_{13}$)

By sintering of mixtures of LiH, Mg, and Os (Ru) powders at up to 833 K under hydrogen pressure between 70 and 155 bar;⁹⁵ powders having light green (low pressure) and grey (high pressure) color; sensitive to air; Os sample pyrophoric; ordered structure (Figure 36) by npd on deuteride of Os compound: $P6_3/mmc$, $Z = 2$; octahedral $[\text{OsH}_6]^{4-}$ 18-electron units having T site symmetry $3m$ surrounded by six Mg^{2+} and two Li^+ in nearly cubic configuration; one Mg and one Li site; three D sites, of which an anionic D^- in trigonal bipyramidal coordination with two

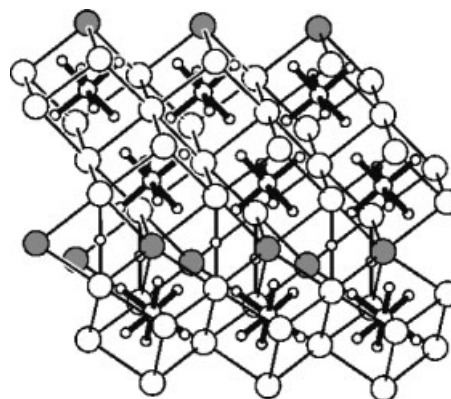


Figure 36 Structure of $\text{LiMg}_4\text{Os}_2\text{D}_{13}$

short linear $\text{Mg}-\text{D}$ and three long triangular $\text{Li}-\text{D}$ bonds; structure derives from Mg_2OsH_6 by intercalation of LiH sheets; intermediate between Mg_2OsH_6 (II) and $\text{LiMg}_2\text{OsH}_7$ (XXVII); lif: $\text{Li}^+ \cdot 4\text{Mg}^{2+} \cdot 2[\text{TH}_6]^{4-} \cdot \text{H}^-$; Os^{II} , d^6 .

Distances (\AA): $\text{Os}-\text{D} = 1.69(3\times)$ and $1.70(3\times)$; $\text{Os}-\text{Li} = 2.69$; $\text{Os}-\text{Mg} = 2.85$; $\text{Mg}-\text{Li} = 3.31$; $\text{Mg}-\text{Mg} = 3.26$; $\text{Li}-\text{D} = 2.13$; $\text{Li}-\text{D}^- = 2.73$; $\text{Mg}-\text{D} = 2.24$; $\text{Mg}-\text{D}^- = 1.87$; $\text{D}-\text{D} = 2.31$.

3.37 Li_2PtH_2

By thermal decomposition of $\text{Li}_5\text{Pt}_2\text{H}_9$ (XXXIV) at 493 K under argon;¹¹⁴ ordered structure (Figure 37) from npd on deuteride: $Immm$, $Z = 2$; contains linear $[\text{PtD}_2]^{2-}$ 14-electron complexes with mmm symmetry; orthorhombic distortion of tetragonal Pd analog Li_2PdH_2 (VII); lif: $2\text{Li}^+ \cdot [\text{PtH}_2]^{2-}$; Pt^0 , d^{10} .

Distances (\AA): $\text{Pt}-\text{D} = 1.64(2\times)$; $\text{Pt}-\text{Pt} = 2.99$; $\text{Pt}-\text{Li} = 2.61$; $\text{Li}-\text{Li} = 2.75$; $\text{Li}-\text{D} = 2.01$; $\text{D}-\text{D} = 2.82$.

3.38 $\text{BaMg}_2\text{RuH}_8$ ($\text{BaMg}_2\text{OsH}_8$)

By sintering powder mixtures of BaMg_2 alloy, BaH_2 , and Ru with LiH flux at temperatures of up to 803 K and H_2 pressures of up to 150 bar;¹¹⁵ greenish powder;

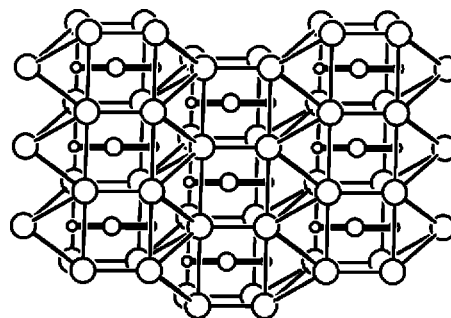


Figure 37 Structure of Li_2PtD_2

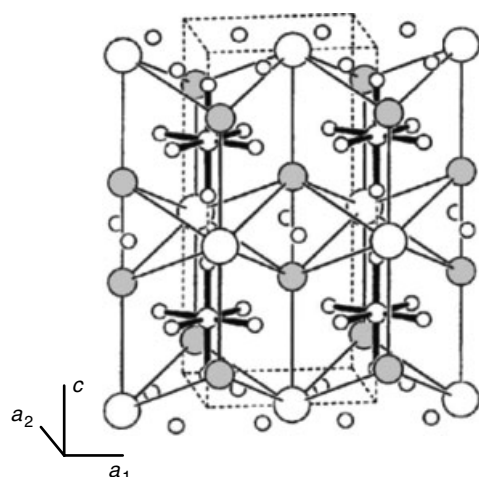


Figure 38 Structure of $\text{BaMg}_2\text{RuD}_8$

Table 18 Interatomic distances (Å) in $\text{BaMg}_2\text{RuD}_8$ and osmium analog

	T = Ru	T = Os
T–D	1.68–1.72	1.70–1.72
T–Mg	2.74	2.75
T–Ba	3.67	3.67
Mg–D	2.10	2.12
Mg–D ⁻	1.99	1.97
Ba–D	2.68	2.68
Ba–D ⁻	2.77	2.77
T–T	4.96	4.97
Mg–Mg	3.08	3.03
Mg–Ba	3.83	3.82
D–D	2.04	2.02

ordered structure (Figure 38) by npd on deuterides of Ru and Os compounds at room temperature: $P4_2/mmc$, $Z = 2$; octahedral $[\text{TH}_6]^{4-}$ 18-electron units having T site symmetry $\bar{4}m2$ surrounded by four Mg^{2+} and four Ba^{2+} forming two interpenetrating tetrahedral; similarity to iron analog $\text{BaMg}_2\text{FeH}_8$ (XVI); three D sites, of which one hydridic D⁻ is tetrahedral coordinated by two Ba and two Mg; lif: $\text{Ba}^{2+} \cdot 2\text{Mg}^{2+} \cdot [\text{TH}_6]^{4-} \cdot 2\text{H}^-$; T^{II}, d⁶. Interatomic distances are given in Table 18.

3.39 NaBaPdH₃

By sintering of compacted powder mixtures of NaH, BaH_2 , and Pd at temperatures of up to 783 K under H_2 pressures of 90 bar;¹¹⁶ solid having metallic luster, sensitive to air and moisture, contains ruby-red single crystals; ordered structure (Figure 39) from single-crystal X-ray diffraction on hydride and npd on deuteride: $P6_3/mmc$, $Z = 2$; contains trigonal planar $[\text{PdH}_3]^{3-}$ 16-electron complexes with $\bar{6}m2$ symmetry; surrounded by five Ba in trigonal bipyramidal configuration; one Pd site, one Na site, one Ba site and one D site;

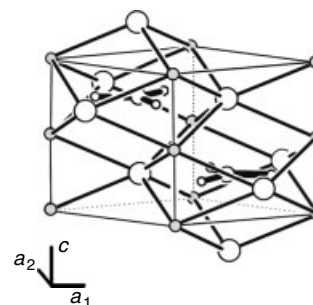


Figure 39 Structure of NaBaPdD_3

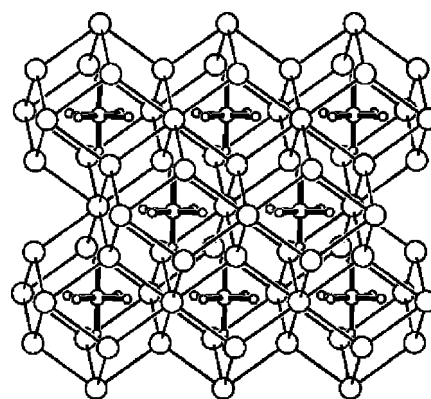


Figure 40 Structure of K_3ReD_6

lif: $\text{Na}^+ \cdot \text{Ba}^{2+} \cdot [\text{PdH}_3]^{3-}$; Pd⁰, d¹⁰ (supported by ac-magnetic susceptibility measurements).

Distances (Å): Pd–D = 1.72(3×); Pd–Ba = 3.04; Pd–Na = 3.81; Pd–Pd = 4.63; Ba–Na = 3.81; Na–Na = 3.04; Na–D = 2.33; Ba–D = 3.03; D–D = 2.98.

3.40 K₃ReH₆

By hydrogenation of powder mixtures of KH and Re at 850 K and H_2 pressures of up to 3500 bar.¹¹⁷ Reaction product has olive green color, is unstable in air and moisture, and decomposes under vacuum; ordered structure (Figure 40) from npd on deuteride: cubic variant of cryolite type (K_2NaAlF_6), $Fm\bar{3}m$, $Z = 4$; Re site forming oct- $[\text{ReH}_6]^{3-}$ 16-electron complexes with site symmetry $m\bar{3}m$; surrounded by 14 K^+ forming a bicapped cuboctahedron (of which the closest K^+ , site K1, in eightfold cubic configuration); lif: $3\text{K}^+ \cdot [\text{ReH}_6]^{3-}$; Re^{III}, d⁴ (consistent with experimentally measured weak temperature independent paramagnetism).

Distances (Å): Re–D = 1.71(6×); Re–D = 3.73; Re–Re = 6.10; K–D = 2.60; K–K = 3.73; D–D = 2.41.

3.41 Ca₈Rh₆H₂₄

From calcium hydride and rhodium metal by sintering powder mixtures at temperatures of up to 1133 K under

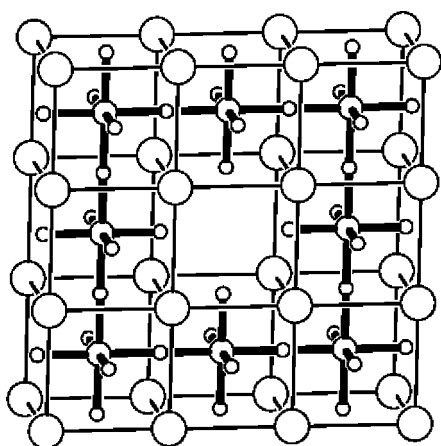


Figure 41 Structure of $\text{Ca}_8\text{Rh}_6\text{D}_{24}$

5 bar hydrogen pressure;⁹³ powder of metallic brass-like appearance, sensitive to moisture and air; ordered structure (Figure 41) closely related to partially disordered more Rh poor $\text{Ca}_8\text{Rh}_5\text{H}_{23}$ (XXVI), intermediate to anion deficient K_2PtCl_6 type (II) and perovskite type; from npd on deuteride: $I\bar{m}\bar{3}m$, $Z = 1$; three-dimensional network of Rh centered, corner-sharing D octahedra (site symmetry $4/m\bar{m}.m$) consisting of four bridging (D2) and two terminal (D1); Ca surrounds octahedra in eightfold cubic configuration; lif: $4n\text{Ca}^{2+} \cdot [\text{Rh}_3\text{H}_{12}]_n^{8n-}$, mixed valence Rh^{1.33'}

Distances (Å): Rh–D = 1.73 (2×) and 1.82 (4×); Rh–Ca = 3.15; Rh–Rh = 3.64; Ca–D = 2.58; Ca–Ca = 3.64; D–D = 2.51.

3.42 $\text{Rb}_3\text{ReH}_{10}$ ($\text{K}_3\text{ReH}_{10}$, $\text{Cs}_3\text{ReH}_{10}$)

By hydrogenation of powder mixtures of alkali hydrides and Re up to 870 K and H_2 pressures of up to 3500 bar (K,^{9,118} Rb,¹¹⁸ Cs¹¹⁹); reaction products are light grey and unstable in air and moisture; disordered structure (Figure 42) from npd on Rb deuteride: cubic room temperature variant:

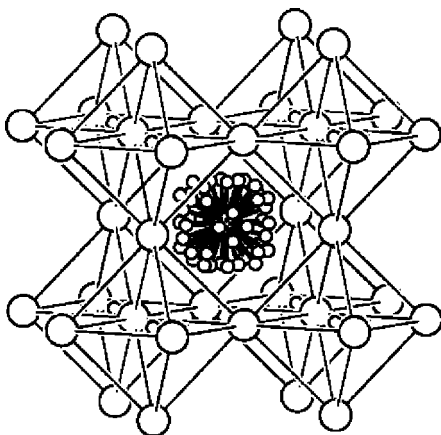


Figure 42 Structure of $\text{Rb}_3\text{ReD}_{10}$

$Pm\bar{3}m$, $Z = 1$; described as ReO_3 type framework containing strongly disordered $[\text{ReH}_9]^{2-}$ 18-electron complexes (average site symmetry $m\bar{3}m$) with two 24-fold disordered D sites (occupancies 0.187 and 0.194), and hydride anions H^- in octahedral M^+ environment; transforms below 110 K into presumably ordered ttp- $[\text{ReH}_9]^{2-}$ complexes (described as ‘monocapped square antiprisms’^{9,118}) having rhombohedral symmetry; lif: $3\text{M}^+ \cdot [\text{ReH}_9]^{2-} \cdot \text{H}^-$; Re^{VII} , d^0 (consistent with experimentally measured diamagnetism on Rb compound).

Distances for disordered structure (Å): Re–D = 1.70 (24×, dis) and 1.71 (24×, disordered); Re–Rb = 4.18; Rb–Rb = 4.18; Re–Re = 6.10; Rb–D = 2.83; Rb–D⁻ = 2.96; D–D = 0.58 (dis).

3.43 Na_3OsH_7 (Na_3RuH_7)

By sintering powder mixtures of NaH and Os (Ru) at temperatures of up to 870 K and H_2 pressures of up to 1500 (Os) and 6000 (Ru) bar.¹²⁰ ordered structure (Figure 43) by npd on deuteride of Os compounds at room temperature: $P4_2/mnm$, $Z = 4$; contains isolated distorted pentagonal bipyramid $[\text{OsH}_7]^{3-}$ 18-electron units having Os site symmetry $m.2m$ surrounded by eight Na^+ (from two Na sites) forming a distorted cube; four D sites; transforms into a HT modification at 459 K; lif: $3\text{Na}^+ \cdot [\text{TH}_7]^{3-}$, T^{IV} , d^4 (supported by experimentally measured weak temperature independent paramagnetism on Os compound). Diffraction evidence¹²⁰ for the existence of cubic phases $\text{M}_{3-\delta}\text{TH}_{7-\delta}$ ($\text{M} = \text{K}, \text{Rb}, \text{Cs}$; $\text{T} = \text{Ru}, \text{Os}$; $\delta \sim 0.12$ for the K–Ru compound).

Distances (Å): Os–D = 1.62–1.70; Na–Os = 3.15; Os–Os = 5.35; Na–D = 2.21; Na–Na = 3.12; D–D = 1.84.

3.44 Cs_3OsH_9 (Rb_3OsH_9)

By sintering powder mixtures of alkali hydrides and Os under conditions similar to Na_3OsH_7 (XLIII).¹²⁰ Partially disordered structure (Figure 44) by npd on deuteride of Cs compound at room temperature: $Pm\bar{3}m$, $Z = 1$; contains

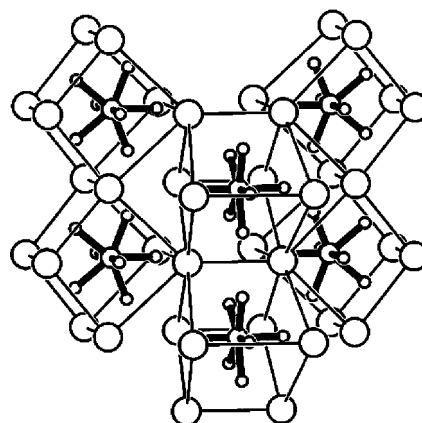


Figure 43 Structure of Na_3OsD_7

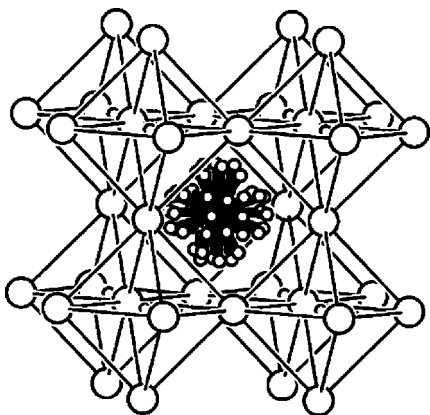


Figure 44 Structure of Cs_3OsD_9

isolated $[\text{OsH}_8]^{3-}$ 18-electron units having strongly disordered D ligands at room temperature as described by two partially occupied 24-fold D sites (occupancy = 1/6, not refined), and one D^- site in octahedral M^+ surrounding; Os (average site symmetry $m\bar{3}m$) surrounded by eight M^+ in cubic configuration; lif: $3\text{M}^+ \cdot [\text{OsH}_8]_{\text{av}}^{2-} \cdot \text{H}^-$; Os^{VI} , d^2 .

Distances (Å): $\text{Os}-\text{D} = 1.59$ (24×, dis) – 1.70 (24×, dis); $\text{Os}-\text{Cs} = 4.33$; $\text{Os}-\text{Os} = 6.13$; $\text{Cs}-\text{D} = 2.91$; $\text{Cs}-\text{D}^- = 3.06$; $\text{Cs}-\text{Cs} = 4.33$; $\text{D}-\text{D} = 0.70$ (dis).

3.45 $\text{Mg}_6\text{Ir}_2\text{H}_{11}$

From either hydrogenated binary Mg_3Ir alloy or by sintering powder mixtures of the elements at up to 773 K under a H_2 pressure of up to 150 bar.¹²¹ Red colored hydride; partially disordered structure (Figure 45) from npd on deuteride; $P2_1/c$, $Z = 8$; contains four symmetry independent Ir hydride complexes: a spy $[\text{IrH}_5]^{4-}$ and three sad $[\text{IrH}_4]^{5-}$ complexes of which two are disordered, and five hydride anions are exclusively bonded to Mg; all complexes are surrounded by Mg in distorted cubic

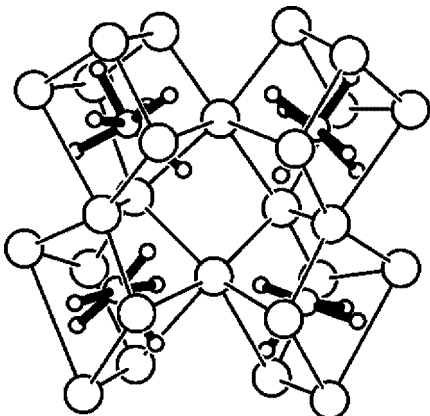


Figure 45 Structure of $\text{Mg}_6\text{Ir}_2\text{D}_{11}$

configurations; metal substructure represents a monoclinic distortion of orthorhombic Co analog $\text{Mg}_6\text{Co}_2\text{D}_{11}$ (XVII); lif: $12\text{Mg}^{2+} \cdot [\text{IrH}_5]^{4-} \cdot [\text{IrH}_4]^{5-} \cdot 2[\text{IrH}_4]_{\text{av}}^{5-} \cdot 5\text{H}^-$; mixed valence Ir^I , d^8 and Ir^{-I} , d^{10} .

Distances (Å): $\text{Ir}1-\text{D} = 1.67-2.07$, $\text{Ir}2-\text{D} = 1.66-1.74$, $\text{Ir}1a-\text{D} = 1.67-1.99$, $\text{Ir}2a-\text{D} = 1.64-1.90$; $\text{Ir}-\text{Mg} = 2.65$; $\text{Ir}-\text{Ir} = 4.62$; $\text{Mg}-\text{Mg} = 2.79$; $\text{Mg}-\text{D} = 1.79$; $\text{Mg}-\text{D}^- = 1.74$; $\text{D}-\text{D} = 2.11$.

3.46 $\text{NdMgNi}_4\text{H}_{3.6}$ ($\text{LaMgNi}_4\text{H}_{\sim 3.6}$)

From hydrogenation of intermetallic compounds NdMgNi_4 and LaMgNi_4 at 323 K under H_2 pressure of up to 7–8 bar;¹²² metallic powders decompose in air by catalytic water formation; nearly ordered structure of $\text{NdMgNi}_4\text{H}_{3.6}$ (Figure 46) from npd on deuteride; $Pnm2_1$, $Z = 4$; contains three Ni sites and three almost fully occupied D sites (occupancies 0.89–0.92) forming $[\text{Ni}_4\text{H}_{\sim 4}]^{5-}$ tetramers in which three edges and one face of the Ni tetrahedron is bridged by hydrogen; tetramers are surrounded by monocapped trigonal prisms formed by four Nd and three Mg; lif: $\text{M}^{3+} \cdot \text{Mg}^{2+} \cdot [\text{Ni}_4\text{H}_{\sim 4}]^{5-}$.

Distances (Å): $\text{Ni}-\text{D} = 1.64-1.72$; $\text{Ni}-\text{Ni} = 2.44$; $\text{Ni}-\text{Mg} = 2.83$; $\text{Ni}-\text{Nd} = 2.90$; $\text{Mg}-\text{Mg} = 4.92$; $\text{Mg}-\text{Nd} = 3.14$; $\text{Mg}-\text{D} = 2.17$; $\text{Nd}-\text{Nd} = 4.98$; $\text{Nd}-\text{D} = 2.34$; $\text{D}-\text{D} = 2.47$.

3.47 $\text{LaMg}_2\text{NiH}_7$

From hydrogenation of ternary metal compound LaMg_2Ni below 473 K under H_2 pressure of up to 8 bar;¹²³ dark grey colored powder sable in air; ordered structure (Figure 47) from npd on deuteride; $P2_1/c$, $Z = 8$; contains two symmetry independent tet- $[\text{NiH}_4]^{4-}$ 18-electron complexes having eight terminal D atoms, and six hydride anions bonded to two Mg and two La only; Ni (site symmetry 1) surrounded by three La (two sites) and six Mg (four sites) in monocapped square antiprismatic configuration;

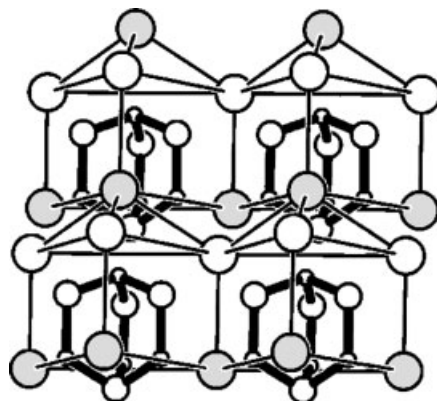


Figure 46 Structure of $\text{NdMgNi}_4\text{D}_{\sim 4}$

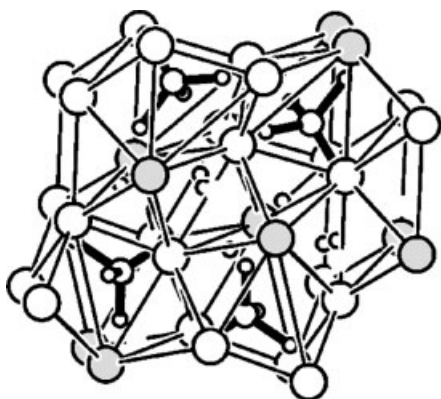


Figure 47 Structure of $\text{LaMg}_2\text{NiD}_7$

lif: $\text{La}^{3+} \cdot 2\text{Mg}^{2+} \cdot [\text{NiH}_4]^{4-} \cdot 3\text{H}^-$; Ni^0 , d^{10} ; hydride is non-metallic; provides example for hydrogenation induced metal (LaMg_2Ni) – to – nonmetal ($\text{LaMg}_2\text{NiH}_7$) transition.

Distances (Å): Ni1–D = 1.49–1.63, Ni2–D = 1.48–1.63; Ni–Mg = 2.59; Ni–La = 3.36; Ni–Ni = 4.14; Mg–Mg = 3.02; Mg–La = 3.42; La–La = 4.06; Mg–D = 1.94; Mg–D⁻ = 1.82; La–D = 2.39; La–D⁻ = 2.33; D–D = 2.12.

4 CRYSTAL CHEMISTRY

4.1 Hydride Complexes

Occurrence. At present, some 50 different homoleptic hydride complexes have been identified in over 127 compounds that cover 47 structure types. Their occurrence across the 3d, 4d, and 5d transition metal series is summarized in Table 19. The complexes form with transition elements from group seven (Mn), eight (Fe), nine (Co) and ten (Ni), to closed d-shell elements of group eleven (Cu) and twelve (Zn). Hydride complexes have not been characterized as yet for elements of group four (Ti), five (V) and six (Cr), and none for Ag, Au, and Hg. Interestingly, most complexes contain T-metals that do not form stable binary hydrides such as iron, cobalt, and congeners, or form relatively unstable hydrides such as nickel and congeners. While the great majority of complexes are centred by one T-metal atom ('mononuclear' complexes) and display terminal hydrogen ligands only, some are centred by two (Ru, Pt), four (Rh, Ni) or more (Ru, Rh) and display both terminal and bridging hydrogen ligands, and/or T–T metal–metal bonds ('polynuclear' complexes).

Mononuclear Complexes. They show at least 10 different geometries that are represented in Table 20. They range from tricapped trigonal prismatic (e.g. $[\text{ReH}_7]^{2-}$), pentagonal bipyramidal (e.g. $[\text{OsH}_7]^{3-}$), octahedral (e.g.

$[\text{FeH}_6]^{4-}$, $[\text{ReH}_6]^{3-}$), square pyramidal (e.g. $[\text{CoH}_5]^{4-}$), planar (e.g. $[\text{RhH}_4]^{3-}$), tetrahedral (e.g. $[\text{NiH}_4]^{4-}$), saddle-like (e.g. $[\text{IrH}_4]^{5-}$), triangular (e.g. $[\text{PdH}_3]^{3-}$), T-shaped (e.g. $[\text{RuH}_3]^{6-}$) to linear (e.g. $[\text{PdH}_2]^{2-}$). Generally speaking, the ligand geometries resemble those of transition metals in 'inorganic molecules'¹²⁴ and coordination compounds such as metal carbonyls and cyanides, and are consistent with conventional electron counts, that is, they are octahedral (usually 18 electrons and d^6), such as $\text{Mo}(\text{CO})_6$; square planar (usually 16 electrons, d^8), such as $\text{Ni}(\text{CN})_4^{2-}$; square pyramidal (18 electrons, d^8), such as $[\text{Ni}(\text{CN})_5]^{3-}$; saddle-like, such as the binuclear nonbridged structure of $\text{Co}_2(\text{CO})_8$ (formally 17 electrons, d^9) or the trinuclear structure of $\text{Ru}_3(\text{CO})_{12}$ (formally 16 electrons, d^8); tetrahedral (usually 18 electrons, d^{10}), such as $\text{Ni}(\text{CO})_4$; or linear (usually 14 electrons, d^{10}), such as the usual ligand geometry of Ag^I (d^{10}) and congeners. Complexes having less than 13 electrons or more than 18 electrons have not yet been reported. The tetrahedral 13-electron $[\text{MnH}_4]^{2-}$ complex in K_3MnH_5 (XXX) is remarkable because it displays a half-filled d shell and leads to a pink colored hydride that orders magnetically. Other interesting cases are the T-shaped formally 17-electron $[\text{RuH}_3]^{6-}$ complex in Mg_3RuH_3 (XV) and the saddle-like formally 16-electron $[\text{RuH}_4]^{4-}$ complex in Mg_2RuH_4 (XVIII), because they provides possible links to polynuclear complexes (see below). Some complex geometries represent only averages such as $[\text{CoH}_4]_{\text{av}}^{5-}$, $[\text{RuH}_5]_{\text{av}}^{5-}$, $[\text{OsH}_8]_{\text{av}}^{2-}$ (not included in Table 20), $[\text{PdH}_3]_{\text{av}}^{3-}$, and $[\text{IrH}_3]_{\text{av}}^{6-}$ (not included in Table 20), because of structural disorder. A five-coordinate trigonal bipyramidal hydrogen configuration similar to the ligand geometry in $\text{Fe}(\text{CO})_5$ has not yet been reported. The presumably square antiprismatic configuration in Cs_3OsH_9 (XLIV) has not yet been ascertained.

Some T-metals adopt one type of ligand geometry only, such as Fe that forms exclusively oct- $[\text{FeH}_6]^{4-}$ complexes (occurring in three hydride structure types, see Table 19), while others adopt two geometries, such as Co that forms sad- $[\text{CoH}_4]^{5-}$ and spy- $[\text{CoH}_5]^{4-}$ complexes (either ordered or disordered), or three or more geometries, such as Ru that forms five: ts- $[\text{RuH}_3]^{6-}$, sad- $[\text{RuH}_4]^{4-}$, spy- $[\text{RuH}_5]_{\text{av}}^{4-}$, oct- $[\text{RuH}_6]^{4-}$, and pbp- $[\text{RuH}_7]^{3-}$. Each hydride structure usually contains one crystallographic T-metal site. Exceptions are K_2ReH_9 (I), $\text{Mg}_6\text{Co}_2\text{H}_{11}$ (XVII), and $\text{LaMg}_2\text{NiH}_7$ (XLVII) that contain two, K_3PdH_3 (IX), $\text{Sr}_8\text{Rh}_5\text{H}_{23}$ (XXVI), and $\text{LaMgNi}_4\text{H}_4$ (XLVI) that contain three, and $\text{Mg}_6\text{Ir}_2\text{H}_{11}$ (XLV) that contains four independent T-metal sites. Among these $\text{Mg}_6\text{Co}_2\text{H}_{11}$ (XVII) and $\text{Mg}_6\text{Ir}_2\text{H}_{11}$ (XLV) are remarkable because the T-metal sites display different complex geometries in the same structure: one sad- $[\text{TH}_4]^{5-}$ and three spy- $[\text{TH}_5]^{4-}$ of which two are disordered (T = Co, Ir). T-metal complexes having a given geometry usually occurs in different structure types such as oct- $[\text{FeH}_6]^{4-}$ in Mg_2FeH_6 (II), $\text{SrMg}_2\text{FeH}_6$ (XVI) and $\text{Ca}_4\text{Mg}_4\text{Fe}_3\text{H}_{22}$ (XX), and tet- $[\text{NiH}_4]^{4-}$ in Mg_2NiH_4 (V) CaMgNiH_4 (XIX) and $\text{LaMg}_2\text{NiH}_7$ (XLVII). Complexes centred by different T-metals in the

Table 19 Homonuclear and polynuclear complex anions as found in various hydride structure types

Mn	Fe	Co	Ni	Cu	Zn
[MnH ₄] ²⁻ XXX [MnH ₆] ⁵⁻ XXIII	[FeH ₆] ⁴⁻ II, XVI, XX	[CoH ₄] ⁵⁻ , XVII [CoH ₄] _{av} ⁵⁻ [CoH ₅] ⁴⁻ III [CoH ₅] _{av} ⁴⁻ XVII, XXXII	[NiH ₄] ⁴⁻ V, XIX, XLVII [Ni ₄ H ₄] ⁵⁻ XLVI [NiH _{3-x}] _{n,av} ²ⁿ⁻ X	[CuH ₄] ³⁻ XXXV	[ZnH ₄] ²⁻ XXIX, XXX
Tc	Ru	Rh	Pd	Ag	Cd
[TcH ₉] ²⁻ I	[Ru ₂ H ₆] ¹²⁻ XV [RuH ₄] _n ⁴ⁿ⁻ XXVIII [RuH ₅] _{av} ⁵⁻ XXV [RuH ₆] ⁴⁻ II, XI, XXVII, XXXVI, XXXVIII [RuH ₇] ³⁻ XLIII	[Rh ₄ H ₄] ⁸⁻ XIV [RhH ₄] ³⁻ XIII [Rh ₃ H ₁₂] _n ⁸ⁿ⁻ XLI [Rh ₄ H ₁₇] _n ¹³ⁿ⁻ XXVI [RhH ₅] _{av} ⁴⁻ III [RhH ₆] ³⁻ XII, XXVI	[PdH ₂] ²⁻ VII, IX [PdH _{2+x}] _{n,av} ²ⁿ⁻ X [PdH ₃] ³⁻ XXXIX [PdH ₃] _{av} ³⁻ XXII [PdH ₄] ²⁻ IV, VI, VIII [PdH ₄] ⁴⁻ XXIX		[CdH ₄] ²⁻ XXX
Re	Os	Ir	Pt	Au	Hg
[ReH ₆] ³⁻ XL [ReH ₆] ⁵⁻ XXIII [ReH ₉] ²⁻ I, XXVIII, XXXIII [ReH ₉] _{av} ²⁻ XLII	[OsH ₆] ⁴⁻ II, XI, XXVII, XXXVI, XXXVIII [OsH ₇] ³⁻ XLIII [OsH ₈] _{av} ²⁻ XLIV	[IrH ₃] _{av} ⁶⁻ XXIV [IrH ₄] ⁵⁻ XLV [IrH ₄] _{av} ⁵⁻ XLV [IrH ₅] ⁴⁻ XLV [IrH ₅] _{av} ⁴⁻ III [IrH ₆] ³⁻ XII, XXXI	[PtH ₂] ²⁻ XXXVII [PtH ₄] ²⁻ IV, VI, VIII, XXI [Pt ₂ H ₉] ⁵⁻ XXXIV [PtH ₆] ²⁻ II		

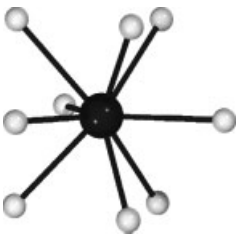
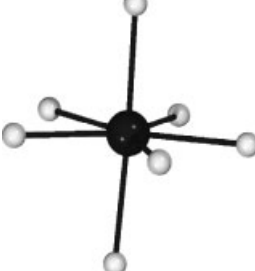
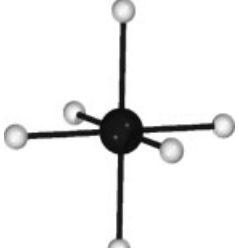
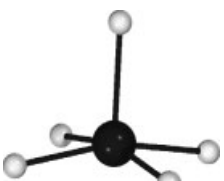



same structure have not yet been reported. ‘Composite’ hydride structures made up by covalent bonded hydride complexes and ionic bonded hydrogen occur with SrMg₂FeH₈ (XVI), Ba₂PtH₆ (XXI), LiSr₂PdH₅ (XXII), Mg₃ReH₇ (XXIII), Mg₃RuH₆ (XXV), LiMg₂RuH₇ (XXVII), LiMg₄Os₂H₁₃ (XXXVI), LaMg₂NiH₇ (XLVII), and can be studied on Figures 16, 21, 22, 23, 25, 27, 36, and 47, respectively. Those belonging to the series LiH·nMg₂TH₄ (T = Ru, Os; n = 1, 2, ∞, groups XXVII, XXXVI, and II, respectively) are made up by slabs of [TH₆]⁴⁻ complexes and sheets of ionic Li⁺H⁻. Finally, only relatively few 3d analogs exist to the more numerous 4d and 5d hydrides, that is, four Mn versus eight Re compounds, five Co versus twelve Rh and ten Ir compounds, and ten Ni versus twenty-one Pd and seventeen Pt compounds. In particular, no iron analog exists for the ruthenium (osmium) series of composite structures, and no nickel analogs exist for any of the palladium and platinum compounds.

Polynuclear Complexes. Dinuclear complexes occur in nonmetallic Li₃Pt₂H₉ (XXXIV) and metallic Mg₃RuH₃ (XV). The former displays planar PtH₄ units that are connected via Pt–H–Pt bridges to [Pt₂H₉]⁵⁻ complexes, and the latter display T-shaped RuH₃ units that are possibly connected via Ru–Ru bonds to [Ru₂H₆]¹²⁻ dimers. Tetranuclear complexes occur in metallic MgRhH_{0.94} (XIV) and NdMgNi₄H_{~4} (XLVI). The former displays cyclic tetramers [Rh₄H_{~4}]⁸⁻ having nearly linear T–H–T bridges, and the latter tetrahedron shaped [Ni₄H_{~4}]⁵⁻ units in which three edges and one face of

the Ni tetrahedron are bridged by hydrogen. Quasi one-dimensional [Ru_nH_{4n}]⁴ⁿ⁻ polymers displaying T–T bonds can be formulated in Mg₂RuH₄ (XVIII), and a two-dimensional disordered [Rh₄H₁₇]_n¹³ⁿ⁻ network of corner-sharing RhH₆ octahedra occurs in Ca₈Rh₅H₂₃ (XXVI). Three-dimensional ordered networks of corner-sharing TH₆ octahedra occur in brass colored Ca₈Rh₆H₂₄ (XLI; [Rh₃H₁₂]_n⁸ⁿ⁻ anion), and the perovskite structure of metallic EuPdH₃ (X; [PdH₃]_n²ⁿ⁻ anion). Polynuclear complexes with mixed T-metals such as in metal carbonyls have not been reported as yet.

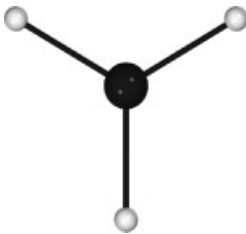
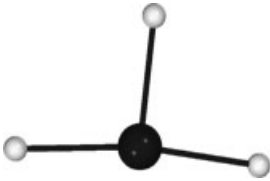

Complex Formation In Intermetallic (‘Interstitial’) Hydrides. The historically first example for a hydrogenation induced complex formation is Mg₂NiH₄ (V). The brownish colored hydride derives by hydrogenation of the intermetallic compound Mg₂Ni and was originally classified as an ‘interstitial’ hydride. It contains an ordered array of [NiH₄]⁴⁻ complexes, is stoichiometric and nonmetallic, and shows a relatively important but reversible rearrangement of its metal atom substructure. Complex formation also occurs in other metal-rich metal framework structures such as the palladium compounds CaPdH₂ (X and analogs) and LiSr₂PdH₅ (XXII). The hydrides have CsCl-type metal substructures and can be described in terms of isolated, partially disordered [PdH₂]_{av}²⁻ and [PdH₃]_{av}³⁻ groups, respectively, but the data are also compatible with 3-dimensional networks of Pd–H–Pd bridges as in ‘interstitial’ hydrides.²³ More palladium rich hydrides based on close-packed metal atom arrangements are NaPd₃H₂¹²⁵ and LiPdH_{0.7}¹²⁶ (not included in this review). While the former shows an ordered array of well-defined linear H–Pd–H

Table 20 Homonuclear transition metal hydride complexes^a and formal electron configurations

	CN Geometry	Complex	Structure types	T	# e-
	9 Tricapped trigonal prismatic	[ReH ₉] ²⁻ [TcH ₉] ²⁻	I, XXVIII, XXXIII, XLII I	d ⁰ d ⁰	18 18
	7 pentagonal bipyramidal	[OsH ₇] ³⁻ [RuH ₇] ³⁻	XLIII XLIII	d ⁶ d ⁶	18 18
	6 octahedral	[MnH ₆] ⁵⁻ [ReH ₆] ⁵⁻ [ReH ₆] ³⁻ [FeH ₆] ⁴⁻ [RuH ₆] ⁴⁻ [OsH ₆] ⁴⁻ [RhH ₆] ³⁻ [IrH ₆] ³⁻ [PtH ₆] ²⁻	XXIII XXIII XL II, XX, XVI II, XI, XXVII, XXXVI XXXVIII II, XI, XXVII, XXXVI XXXVIII XII, XXVI XII, XXXI II	d ⁶ d ⁶ d ⁴ d ⁶ d ⁶ d ⁶ d ⁶ d ⁶ d ⁶	18 18 16 18 18 18 18 18 18
	5 square pyramidal	[RuH ₅] _{av} ⁵⁻ [CoH ₅] ⁴⁻ [CoH ₅] _{av} ⁴⁻ [IrH ₅] ⁴⁻ [IrH ₅] _{av} ⁴⁻	XXV III XVII, XXXII XLV III, XLV	d ⁸ av d ⁸ d ⁸ av d ⁸ d ⁸ av	18 18 18 18 18
	4 square planar	[RhH ₄] ³⁻ [PdH ₄] ²⁻ [PtH ₄] ²⁻	XIII IV, VII, VIII VII, VIII, XXI	d ⁸ d ⁸ d ⁸	16 16 16
	4 tetrahedral	[MnH ₄] ²⁻ [NiH ₄] ⁴⁻ [PdH ₄] ⁴⁻ [CuH ₄] ³⁻ [ZnH ₄] ²⁻ [CdH ₄] ²⁻	XXX V, XIX, XLVI XXIX XXXV XXIX, XXX XXX	d ⁵ d ¹⁰ d ¹⁰ d ¹⁰ d ¹⁰ d ¹⁰	13 18 18 18 18 18
	4 saddle-like	[CoH ₄] ⁵⁻ [RuH ₄] ⁴⁻ [IrH ₄] ⁵⁻	XVII XVIII XLV	d ¹⁰ d ⁸ d ¹⁰	18 16 18

(cont'd overleaf)

Table 20 cont'd

	CN Geometry	Complex	Structure types	T	# e-
	3 triangular	$[\text{PdH}_3]^{3-}$	XXXIX	d^{10}	16
	3 T-shaped	$[\text{RuH}_3]^{6-}$ $[\text{PdH}_3]_{\text{av}}^{3-}$	XV XXII	Dimer d^{10} av	17 16
	2 linear	$[\text{PdH}_2]^{2-}$ $[\text{PdH}_2]_{\text{av}}^{2-}$ $[\text{PtH}_2]^{2-}$	VI, IX X XXXVII	d^{10} d^{10} av d^{10}	14 14 14

^aIn decreasing coordination number, CN; only structurally characterized, essentially ordered monomers having terminal H ligands are included; av: average due to disorder.

groups, the latter is disordered and shows only a weak tendency for complex formation. As to the above mentioned metallic hydrides $\text{MgRhH}_{\sim 0.9}$ (XIV) and $\text{NdMgNi}_4\text{H}_{\sim 4}$ (XLVI), their hydrogen distributions can be described as ‘interstitial’, but the stereochemical activity of the tetramers $[\text{Rh}_4\text{H}_4]^{8-}$ and $[\text{Ni}_4\text{H}_4]^{5-}$, respectively, is evident. These findings suggest that hydride complex formation could be a general phenomenon in interstitial hydrides, at least on a local level. Some striking examples for hydrogenation induced complex formations and metal-insulator transitions have been recently reported in the systems $\text{Mg}_3\text{Ir}-\text{H}_2$ ¹²¹ and $\text{LaMg}_2\text{Ni}-\text{H}_2$.¹²³ The former contains the intensely red colored hydride $\text{Mg}_6\text{Ir}_2\text{H}_{11}$ (XLV) the structure of which can be rationalized in terms of pyr- $[\text{IrH}_5]^{4-}$ and sad- $[\text{IrH}_4]^{5-}$ 18-electron complexes and hydride anions H^- , in agreement with the limiting ionic formula $4\text{Mg}_6\text{Ir}_2\text{H}_{11} = 5\text{MgH}_2 \cdot 19\text{Mg}^{2+} \cdot 2[\text{IrH}_5]^{4-} \cdot 6[\text{IrH}_4]^{5-}$. The latter contains the grey colored hydride $\text{LaMg}_2\text{NiH}_7$ (XLVII) that is nonmetallic. Its structure contains tetrahedral $[\text{NiH}_4]^{4-}$ complexes and hydride anions H^- corresponding to the limiting ionic formula $\text{LaH}_3 \cdot 2\text{Mg}^{+2} \cdot [\text{NiH}_4]^{4-}$. Thus both compounds can be considered as ‘complex’ hydrides for which the ‘interstitial’ concept fails.

Order–Disorder Transitions. The mobility of the hydrogen ligands (or of the entire complexes) at room temperature is generally high. Well-characterized order–disorder transitions within the complexes near room temperature occur in Mg_2CoH_5 (III), Mg_2NiH_4 (V), K_3PdH_3 (IX), Na_2PtH_4 (IV), M_3PtH_5 (M = Rb, Cs; VIII), and M_2PtH_4 (M = K, Rb, Cs; VI). Complexes that are partially disordered at room temperature and do not readily order at low temperature occur in CaPdH_2 (X), $\text{LiSr}_2\text{PdH}_5$ (XXII), Mg_4IrD_5 (XXIV), Mg_3RuH_6

(XXV), M_2TH_5 (T = Rh, Ir; M = Mg, Ca, Sr, Eu; III) and $\text{Mg}_6\text{T}_2\text{H}_{11}$ (T = Co; XVII, and Ir; XLV). In some structures, the hydride complexes undergo rigid motions, such as in K_2PtH_4 for which LT-NMR data suggest rotational jumps of the spl-PtH₄ units in the plane of the square.⁸

4.2 Cation Configurations

The cations M (alkali, alkaline earth, lanthanide) surrounding the complexes have various configurations, of which the eightfold cubic (or approximately cubic) is by far the most common. Depending on the metal ratios M/T the cubes are joined via corners, edges, or faces. Edge sharing occurs in Sr_2RuH_6 (II), Sr_2IrH_5 (III), Na_2PtH_4 (IV), Mg_2NiH_4 (V), K_2PtH_4 (VI), and K_3ReH_6 (XL) that adopt one arrangement, and $\text{Ca}_4\text{Mg}_4\text{Fe}_3\text{H}_{22}$ (XX) and $\text{Ca}_4\text{Mg}_4\text{Co}_3\text{H}_{19}$ (XXXII) that adopt another. Corner sharing occurs in Li_4RuH_6 (XI). Corner and edge sharing occurs in Mg_3ReH_7 (XXIII), $\text{Mg}_6\text{Co}_2\text{H}_{11}$ (XVII), Mg_3RuH_6 (XXV), $\text{LiMg}_2\text{RuH}_7$ (XXVII), and $\text{Mg}_6\text{Ir}_2\text{H}_{11}$ (XLV) that adopt one arrangement, and $\text{Sr}_2\text{MgFeH}_8$ (XVI), $\text{LiMg}_4\text{Os}_2\text{H}_{13}$ (XXXVI), and $\text{LiMg}_4\text{Os}_2\text{H}_{13}$ (XXXVI) that adopt another. Sheets of face-sharing cubes occur in Mg_2RuH_4 (XVIII) and $\text{Ba}_3\text{Ir}_2\text{H}_{12}$ (XXXI) for which the sheets are connected via edges, and in $\text{LiSr}_2\text{PdH}_5$ (XXII) for which the sheets are connected via additional M atoms, and in Na_2PdH_2 (VII), Ba_2PtH_6 (XXI), and Li_2PtH_2 (XXXVII) that have other arrangements. Three-dimensional arrays of face-sharing cubes occur in CaPdH_2 (X) and MgRhH_{1-x} (XIV) where all faces are shared, in $\text{Sr}_8\text{Rh}_5\text{H}_{23}$ (XXVI) where edges, edges and faces, or faces are shared, and in $\text{Ca}_8\text{Rh}_6\text{H}_{24}$ (XLI) where edges and faces are

shared. Face-sharing configurations are of particular interest because they favor interactions between neighboring hydride complexes.

The distortion of the M cube depends mainly on the symmetry and dynamics of the hydrido complex. This can be seen in Mg_2CoH_5 (III) and Mg_2NiH_4 (V), whose T-metal centered Mg cubes are regular in the disordered cubic HT structure (such as in Mg_2FeH_6 ; II), and strongly distorted in the tetragonal (Mg_2CoH_5) and monoclinic (Mg_2NiH_4) LT structures owing to ordering of the *spy*- CoH_5 and tet- NiH_4 units, respectively. Another example is Mg_2RuH_4 (XVIII) whose Mg cubes surrounding the *sad*- RuH_4 units are strongly distorted compared to the regular Mg cubes surrounding the *oct*- RuH_6 units in Mg_2RuH_6 (II). The influence of the complex geometry on the metal atom array is also apparent in $\text{Mg}_6\text{Co}_2\text{H}_{11}$ (XVII), $\text{Mg}_6\text{Ir}_2\text{H}_{11}$ (XLV), and Mg_3RuH_6 (XXV). They contain various nonoctahedral TH_4 and TH_5 units, and their metal substructure derives from that of trigonal Mg_3ReH_7 (XXIII) containing octahedral ReH_6 units by an orthorhombic (or monoclinic) distortion. Finally, the atomic size difference between alkaline earths also plays a role, as can be seen from the severe distortions of the partially substituted M cubes in the quaternary hydrides $\text{Ca}_4\text{Mg}_4\text{Fe}_3\text{H}_{22}$ (XX) and CaMgNiH_4 (XIX) that derive from Mg_2FeH_6 (II) and Mg_2NiH_4 (V), respectively.

4.3 Bond Distances

Metal–Hydrogen Bonds. The T–H bond distances of the complexes can be rationalized in terms of covalent radii and a fixed hydrogen radius of 0.28 Å. The distances range from 1.50–1.60 Å for 3d metals, to 1.70–1.80 Å for 4d and 5d metals, except for Pd (1.60–1.70 Å) and Pt (1.58–1.67 Å), the T–H bonds of which are shortened owing to low-coordination numbers. Apparent bond shortening may also occur as a result of partial hydrogen site occupancy in disordered HT structures. On the other hand, the relatively long Pd–D distances in disordered CaPdD_2 (X) (Pd–D = 1.84 Å) and $\text{LiSr}_2\text{PdD}_5$ (XXII) (Pd–D = 1.95 Å) are only averages, and are presumably shortened locally owing to the formation of linear PdD_2 groups. Owing to matrix effects,¹²⁷ the T–D bond lengths generally increase with the size of the M cations.

The M–H distances are consistent with tabulated ionic radii. Those involving hydride anions H^- surrounded by cations M only (occurring in some 25 compounds from 19 different structure types) are generally shorter than those involving hydrogen ligands of the complex. Exceptions are found in K_3PdH_3 (IX), K_3ZnH_5 and K_3MnH_5 (XXX), $\text{Ba}_7\text{Cu}_3\text{H}_{17}$ (XXXV), $\text{Rb}_3\text{ReH}_{10}$ (XLII), and Cs_3OsH_9 (XLIV). Unlike the complex hydrogen ligands, the hydride anions are neither mobile nor disordered. Their metal configurations range from octahedral in $\text{LiSr}_2\text{PdH}_5$ (XXII), K_3PdD_3 (IX), K_3ZnH_5 (XXX), $\text{Rb}_3\text{ReH}_{10}$ (XLII),

Cs_3OsH_9 (XLIV), and $\text{LaMg}_2\text{NiH}_7$ (XLVII), to trigonal bipyramidal in $\text{LiMg}_2\text{RuH}_7$ (XXVII) and $\text{LiMg}_4\text{Os}_2\text{H}_{13}$ (XXXVI), tetrahedral in $\text{SrMg}_2\text{FeH}_8$ (XVI), $\text{Ca}_4\text{Mg}_4\text{Fe}_3\text{H}_{22}$ (XX), $\text{Ca}_4\text{Mg}_4\text{Co}_3\text{H}_{19}$ (XXXII), $\text{Ba}_7\text{Cu}_3\text{H}_{17}$ (XXXV), and $\text{BaMg}_2\text{RuH}_8$ (XXXVIII), triangular in $\text{Mg}_6\text{Co}_2\text{H}_{11}$ (XVII) and $\text{LaMg}_2\text{NiH}_7$ (XLVII), and linear in Mg_3ReH_7 (XXIII) and Mg_3RuH_6 (XXV). As expected, low-coordinate M–H bonds are significantly shorter, for example, Mg–H = 1.74 Å in $\text{Mg}_6\text{Ir}_2\text{H}_{11}$ (XLV) and K–H = 2.73 Å in K_3PdH_5 (VIII) compared to higher coordinate M–H bonds such as in binary MgH_2 (1.95 Å), BaH_2 (2.57 Å) and KH (2.85 Å). As in saline ternary hydrides, the Yb–D distances are close to Ca–D distances and the Eu–D distances close to Sr–D distances.¹²⁸

Metal–Metal Bonds. The T- and M-metals are likely to interact in complex hydride structures because of their proximity. The shortest M–T distances are in the range 2.5–3.5 Å and give rise to metallic properties in metal-rich compounds, such as MgRhD_{1-x} (XIV) (Mg–Rh = 2.66 Å) and Na_2PdH_2 (VII) (Na–Pd = 3.13 Å). The shortest M–M distances are in the range 2.5–4.5 Å and come close to the sum of covalent radii, such as Mg–Mg = 2.75 Å in Mg_4IrH_5 (XXIV), 2.78 Å in $\text{Mg}_6\text{Co}_2\text{H}_{11}$ (XVII) or 2.79 Å in $\text{Mg}_6\text{Ir}_2\text{H}_{11}$ (XLV). Clearly, these M–T and M–M interactions are not taken into account by a limiting ionic bond description and require more sophisticated electron counting schemes (see 4.4). Interactions between T-atoms are less common, because the T–T distances usually exceed 3.5 Å. However, T–T interactions do occur in metallic Li_2PdH_2 (VII) (Pd–Pd = 3.11 Å) and Na_2PdH_2 (VII) (Pd–Pd = 3.60 Å), and possibly also in Mg_2RuH_4 (XVIII) (Ru–Ru = 3.24 Å) and Mg_3RuH_3 (XV) (Ru–Ru = 3.31 Å) as suggested by their stereochemistry and the existence of carbonyls displaying such interactions across similar long distances.

Hydrogen–Hydrogen Contacts. The H–H contacts in ordered hydride structures usually exceed 2.1 Å, and thus indicate nonbonding (or repulsive) H–H interactions. In disordered structures, H sites closer than 2.1 Å are always half (or less) occupied. The shortest H–H contact occurs in K_2ReD_9 (I) for which the most recently reported value is D–D = 1.90 Å.²⁴ Thus, there is no evidence for hydrogen pairing in homoleptic solid-state T-metal hydrides, unlike in molecular T-metal hydride complexes for which dihydrogen groups with H–H distances as short as 0.82 Å do occur.^{10,129}

4.4 Bonding

The compositions and ligand geometries of most mononuclear T-metal hydride complexes can be rationalized in terms of conventional electron counts based on full charge

transfer from the surrounding cation matrix M, and s-p-d hybridization schemes that involve two-center-two-electron (2c–2e) bonds, such as $(d^0)d^5sp^3$ for 18-electron ttp-[ReH₉]²⁻, $(d^6)d^2sp^3$ for octahedral 18-electron [FeH₆]⁴⁻, [MnH₆]⁵⁻, and [ReH₆]⁵⁻, $(d^8)dsp^3$ for square-pyramidal 18-electron [CoH₅]⁴⁻, $(d^{10})sp^3$ for 18-electron tetrahedral [NiH₄]⁴⁻ and [PdH₄]⁴⁻, $(d^8)dsp^2$ for planar 16-electron [PdH₄]²⁻ and [RhH₄]³⁻, $(d^{10})sp^2$ for triangular 16-electron [PdH₃]³⁻, and $(d^{10})sp$ for linear 14-electron [PdH₂]²⁻. However, for some hydrides, in particular those containing early T-metals and/or showing metal–metal interactions, more elaborate electron counting schemes evoking s-d hybridization only, three-center-four-electron (3c–4e) bonds, and partial charge transfer from the cation matrix M are also possible, as was shown by Firman and Landis.¹³ Mg₂CoH₅ (III), for example, can be formulated in terms of univalent Mg⁺ and sd² hybridized 16-electron [CoH₃ 2H⁻] complexes having two 3c–4e bonds. The merits and limitations of this bonding model have been discussed by King.¹⁶ For polynuclear hydride complexes, the bonding situation is more difficult to describe. Some can be rationalized by mixtures between two-center-two-electron and three-center-two-electron (3c–2e) bonds, such as dinuclear [H₄Pt–H–PtH₄]⁵⁻ in Li₅Pt₂H₉ (XXXIV) for which eight 2c–2e bonds (terminal H's) and one 3c–2e bond (bridging H) can be formulated, while for others such as tetranuclear [Ni₄H_{~4}]⁵⁻ in LaMgNi₄H_{~4} (XLVI) a similar bond description is less apparent.

As expected from its small atomic size and high-field ligand character, hydrogen favors 18-electron complexes (about 40 representatives with groups 7, 8, 9, and 10 elements). Complexes with 16 electrons (some 11 representatives with Re, Ru, Rh, Pd, and Pt), or 14 electrons (4 representatives with Pd and Pt) are less numerous. The only octahedral 16 electron $(d^4)d^2sp^3$ bonded complex is [ReH₆]³⁻ in K₃ReH₆ (XL), and the only tetrahedral 13-electron $(d^5)sp^3$ bonded complex is [MnH₄]²⁻ in K₃MnH₅ (XXX) that displays a half-filled d shell. On the other hand, the relative softness of hydrogen as a ligand and its stability as an anion favors structural diversity. This is illustrated by 'composite' hydrides such as quaternary Ca₄Mg₄Fe₃H₂₂ (XX) that derives from ternary Mg₂FeH₆ (II) by partial substitution of a fourfold negative [FeH₆]⁴⁻ by four H⁻, and Mg₃ReH₇ (XXIII), Mg₆Co₂H₁₁ (XVII), and Mg₃RuH₆ (XXV) that have a common metal substructure and are capable of accommodating various complex geometries and H⁻ ions.

The formal oxidation numbers of the T-metal in most hydride structures range between –I (Co, Rh), zero (Ru, Ni, Pd), I (Mn, Re, Co, Ir, Rh, Cu), II (Fe, Ru, Os, Pd, Pt, Zn), III (Ir, Rh), IV (Ru, Os, Pt), VI (Os) and VII (Re). They are consistent with configurational differences as found, for example, in palladates that change from tetrahedral as in [Pd⁰H₄]⁴⁻ to planar as in [Pd^{II}H₄]²⁻. As expected, high formal oxidation numbers occur mainly with heavier T elements such as Re^{VII} in [ReH₉]²⁻, Os^{VI} in [OsH₈]²⁻,

and Pt^{IV} in [PtH₆]²⁻, for which no 3d analogs exist. As the H/M ratios decrease, the systems tend to become metallic and electron counting becomes less obvious. Illustrative examples are Mg₃RuH₃ (XV) and Mg₄IrH₅ (XXIV) for which the neglect of Mg–Mg bonding leads to unreasonable electron configurations and formal oxidation numbers (–III for Ru and Ir). Clearly, limiting ionic formulas for such hydrides are misleading, at least from a bonding point of view, but they are still useful for rationalizing hydrogen contents, which is generally not possible with 'interstitial' (metallic) metal hydrides.

Finally, an important bonding feature of complex metal hydrides are the interactions between the complex hydrogen ligands and the surrounding cation matrix. As can be seen from the isoelectronic series Mg₂FeH₆ – Mg₂CoH₅ – Mg₂NiH₄, the cations adopt cubic – or nearly cubic – configurations that maximize the Mg–H interactions. Clearly such M–H interactions not only help stabilizing the complexes but also contribute to the thermal stability of the overall structure, as shown by the desorption enthalpies of substitution pairs such as Mg₂NiH₄–CaMgNiH₄ and Mg₂FeH₆–Ca₄Mg₄Fe₃H₂₂ (see Section 5). On the other hand, T–H interactions do not much contribute to thermal stability as suggested by the relatively weak force constants as measured in metal hydrides such as Mg₂FeH₆ (Fe–H stretching mode ~1.9 mdyne Å⁻¹; Fe–H = 1.56 Å),³⁸ and the significant elongation of the T–H bonds in the thermally more stable analog Ca₂FeH₆ (Fe–H = 1.62 Å). Theoretical band structure calculations are available for some of these systems, for example, Mg₃MnH₇ (XXIII),⁹⁰ Na₂PdH₄ (IV), Na₂PdH₂ (VII), Li₂PdH₂ (VII), NaBaPdH₃ (XXXIX), and Ba₂PdH₄ (XXIX),¹⁴ Mg₂NiH₄ (V), Mg₂CoH₅ (III), Mg₂TH₆ (II; T = Fe, Ru, Os), M₂FeH₆ (II; M = Mg, Ca, Sr),³⁷ APdH₃ (X; A = Sr, Eu, Yb),⁷¹ BaReH₉ (XXVIII),⁹⁸ and Eu₂PdH₄ (XXIX),¹⁰³ but have not yet addressed the issue of thermal stability.

5 PROPERTIES

In contrast to their 'interstitial' counterparts, complex metal hydrides have no apparent homogeneity range and are usually nonmetallic. Many are colored (greenish: Mg₂FeH₆, Na₄RuH₆, SrMg₂FeH₈, LiSr₂PdH₅; reddish: Eu₂RuH₆, Mg₂RuH₄; red-violet: Na₂PtH₄; yellow: K₃PdH₃; yellow-green: K₂PdH₄; brownish: Mg₂RuH₆, Mg₂NiH₄, Mg₃RuH₆, Ca₄Mg₄Fe₃H₂₂, BaMg₂FeH₈), while some are colorless (K₂PtH₄, K₃PtH₅, Na₃RhH₆), or appear as white (Mg₂OsH₆, Li₄RuH₆) or gray powders (Ca₂RuH₆, Mg₃RuH₃, Mg₃ReH₇). Only few are black (Yb₂RuH₆, Mg₆Co₂H₁₁, Mg₂CoH₅, YbMgNiH₄, Yb₄Mg₄Fe₃H₂₂) or have metallic luster (Li₃RhH₄, Na₂PdH₂). Relatively well-characterized complex hydrides having metallic properties are Li₂PdH₂ and Na₂PdH₂ that are considered to be two-dimensional metals.

Among complex hydrides that derive from intermetallic compounds, some show hydrogenation induced metal to nonmetal transitions such as brownish-red Mg_2NiH_4 (Mg_2Ni), red $\text{Mg}_6\text{Ir}_2\text{H}_{11}$ (Mg_3Ir), and dark grey $\text{LaMg}_2\text{NiH}_7$ (LaMg_2Ni). Such transitions are of both fundamental and technological interest as shown for binary systems like Y-H_2 (switchable mirrors) and ternary systems like $\text{Mg}_2\text{Ni-H}_2$ (tuneable optic windows).¹³⁰

Many hydrides are diamagnetic, as expected for closed-electron shells associated with low-spin d^6 (oct), d^8 (spl), and d^{10} (tet, lin) configurations. Others show weak temperature independent paramagnetism such as the d^4 systems K_3ReH_6 (XL) and Na_3OsH_7 (XLIII). Finally, systems containing magnetic ions tend to order magnetically at low temperature, such as rose colored K_3MnH_5 (Mn(II), $\mu_{\text{eff}} = 4.5\mu_{\text{B}}$, $T_{\text{N}} = 28\text{ K}$) and faint violet colored Eu_2PdH_4 (Eu(II), $\mu_{\text{eff}} = 8\mu_{\text{B}}$, $T_{\text{C}} = 15\text{ K}$).

Vibrational spectra as measured by INS on hydrides such as M_2TH_6 (II, M = Mg, Ca, Sr, Ba; T = Fe, Ru, Os),^{28,38} Mg_2NiH_4 (V) and Rb_3ZnH_5 (XXX)⁵⁴ indicate T-H stretching and bending modes in the expected ranges of $1600\text{--}2000\text{ cm}^{-1}$ and $800\text{--}1000\text{ cm}^{-1}$, respectively. These modes correlate with bonding properties, such as the T-H stretching frequencies in the K_2PtCl_6 type series (II) that increase in the sequence T = Fe, Ru, Os, and decrease as the M-H bond lengths increase. Their theoretical band gaps show the opposite trend, that is, they increase in the sequence Mg_2TH_6 (T = Fe, Ru, Os) owing to the increasing atomic number of T, and that decrease in the sequence M_2FeH_6 (M = Mg, Ca, Sr) owing to the increased participation of M d orbitals.

Properties of relevance for hydrogen storage applications, such as desorption enthalpies and weight and volume efficiencies, are summarized in Table 21.

Clearly, some compounds have outstanding properties, such as Mg_2FeH_6 , which shows the highest known volume efficiency for hydrogen storage of all materials known ($120\text{ g H}_2\text{ L}^{-1}$, that is, more than twice that of liquid

hydrogen), and BaReH_9 , which has an H/M ratio that surpasses the hydrogen-to-carbon ratio of methane ($\text{H/C} = 4$). The weight efficiencies are also remarkable as shown by Mg_2FeH_6 and Mg_3MnH_7 , which can store up to 5 wt% hydrogen, that is, more than currently used interstitial hydrides such as $\text{AB}_5\text{H}_{\sim 6}$ (A = La, etc., B = Ni, etc.) and $\text{AB}_2\text{H}_{\sim 4}$ (A = Ti, etc., B = Mn, etc.), which store only up to $\sim 2\text{ wt}\%$ hydrogen. Unfortunately, regarding thermal stability complex metal hydrides perform less well than their interstitial counterparts. Only few hydrides decompose near room temperature such as BaReH_9 and $\text{Ba}_7\text{Cu}_3\text{H}_{17}$ that are, however, relatively heavy and expensive and not completely reversible. Mg_2NiH_4 , which is the only commercialized hydride of this class, decomposes only above 523 K, corresponding to a desorption enthalpy of $\Delta H = 64\text{ kJ mol}^{-1}\text{ H}_2$. Most other complex metal hydrides are more stable (decomposition temperatures $> 573\text{ K}$, $\Delta H > 80\text{ kJ/H}_2$) and must be heated to yield hydrogen at useful pressures, which represents a penalty in energy. On the other hand, compounds such as Mg_2FeH_6 are of interest for high-temperature applications³⁹ because of their high thermal stability and ease of cycling.

Owing to the scarcity of thermodynamic data, empirical models such as that used to rationalize thermal stabilities of interstitial metal hydrides¹³¹ do not exist for complex metal hydrides. Metal-hydrogen interactions obviously play a role, as can be seen from the substitution pairs $\text{Mg}_2\text{NiH}_4\text{--CaMgNiH}_4$ and $\text{Mg}_2\text{FeH}_6\text{--Ca}_4\text{Mg}_4\text{Fe}_3\text{H}_{22}$, whose stabilities increase strongly as one goes from the ternary Mg compounds to the quaternary Ca compounds (see Table 21). This trend correlates with the relatively strong interactions between hydrogen and calcium that forms a very stable binary hydride, compared to the relatively weak interactions of hydrogen with magnesium that forms a less stable binary hydride. This suggests that interactions between hydrogen and metal cations govern to a large extent the thermal stability of complex metal hydrides.

Table 21 Desorption enthalpies and hydrogen storage efficiencies

	ΔH $\text{kJ mol}^{-1}\text{ H}_2$	Weight efficiency wt%	Volume efficiency gH_2L^{-1}
Complex hydrides			
Mg_2NiH_4	64	3.6	18
Mg_2CoH_5	86	4.5	126
Mg_2FeH_6	98	5.5	150
CaMgNiH_4	129	3.2	87
$\text{Ca}_4\text{Mg}_4\text{Fe}_3\text{H}_{22}$	122	5.0	121
Binary hydrides			
MgH_2	74	7.7	109
CaH_2	184 ^a	4.8	92
Metallic hydride			
LaNi_5H_6	31	1.4	93

^aModel prediction.¹³¹

6 CONCLUSIONS

Solid-state transition metal hydride complexes occur mainly with the late transition elements. The complexes are usually mononuclear (centred by one T-metal atom only) and contain between two and nine terminal hydrogen ligands, while some are polynuclear (centred by more than one T-metal atom) and display bridging hydrogen ligands. The ligands tend to be disordered at higher temperatures and ordered at lower temperatures. The structural and electronic configurations of the hydrido complexes are consistent with those usually found in coordination compounds. They are stabilized by charge transfer from the surrounding cation matrix, are often 18-electron, and less often 16- or 14-electron. Some hydride structures show evidence for metal-metal interactions, as

in typically interstitial metal hydrides, while others contain additional hydride anions (H^-) bonded to electropositive metals only, such as in saline hydrides. In metal-rich systems, hydrogen has interstitial character, as in typically metallic transition metal hydrides. No H–H bond formation is observed. Most complex hydride systems are nonmetallic and many are colored. Some systems, however, show hydrogenation induced complex formation and metal-to-insulator transitions. They generally display very high volume efficiencies for hydrogen storage but are thermally too stable and/or too expensive for practical applications. Thermodynamic data suggest that their enthalpy of formation scales with the thermal stability of the binary hydrides of the electropositive metal constituents.

7 RELATED ARTICLES

Hydride Complexes of the Transition Metals.

8 REFERENCES

1. K. Yvon, Hydrides: Solid State Transition Metal Complexes, in 'Encyclopedia Inorganic Chemistry', ed. R. B. King, John Wiley, New York 1994, Vol. 3, p. 1401.
2. S. C. Abrahams, A. P. Ginsberg, and K. Knox, *Inorg. Chem.*, 1964, **3**, 558; see also K. Knox and A. P. Ginsberg, *Inorg. Chem.*, 1964, **3**, 555; for K_2TcH_9 see also A. P. Ginsberg, *Inorg. Chem.*, 1964, **3**, 567.
3. R. O. Moyer Jr, C. Stanitski, J. Tanaka, M. I. Kay, and R. Kleinberg, *J. Solid State Chem.*, 1971, **3**, 541; for a review of work by these authors see R. O. Moyer Jr, R. Lindsay, and D. N. Marks, *Adv. Chem. Ser.*, 1978, **167**, 366.
4. L. Schlapbach, *Top. Appl. Phys.*, 1988, **63**, 1; 1992, **67**, 1; see also *MRS Bull.*, 2002, **27/9**, 675.
5. J. J. Reilly and R. H. Wiswall, *Inorg. Chem.*, 1968, **7**, 2254.
6. P. Zolliker, K. Yvon, J. D. Jorgensen, and F. J. Rotella, *Inorg. Chem.*, 1986, **25**, 3590; see also K. Yvon, J. Schefer, and F. Stucki, *Inorg. Chem.*, 1981, **20**, 2776.
7. W. Bronger, *Angew. Chem., Int. Ed. Engl.*, 1991, **30**, 759.
8. W. Bronger, *J. Alloys Comp.*, 1995, **229**, 1.
9. W. Bronger and G. Auffermann, *Chem. Mater.*, 1998, **10**, 2723.
10. R. Bau and M. H. Drabnis, *Inorg. Chim. Acta*, 1997, **259**, 27.
11. K. Yvon, *Z. Kristallogr.*, 2003, **218**, 108.
12. G. J. Miller, H. Deng, and R. Hoffmann, *Inorg. Chem.*, 1994, **33**, 1330.
13. T. K. Firman and C. R. Landis, *J. Am. Chem. Soc.*, 1998, **120**, 12650.
14. M. Olofsson-Martensson, U. Häussermann, J. Tomkinson, and D. Noréus, *J. Am. Chem. Soc.*, 2000, **122**, 6960.
15. K. Yvon, *Chimia*, 1998, **52**, 613.
16. R. B. King, *Coord. Chem. Rev.*, 2000, **200–202**, 813.
17. K. Yvon, *Swiss Neutron News*, 2002, **22**, 11.
18. K. Yvon, 'Encyclopedia of Materials: Science and Technology Updates', ed. K. H. J. Buschow, Elsevier Ltd., 2004, pp. 1–9.
19. W. Grochala and P. P. Edwards, *Chem. Rev.*, 2004, **104**, 1283.
20. G. Sandrock, and G. Thomas, 1997, Hydrogen Information Center, <http://hydpark.ca.sandia.gov/>, IEA/DOE/SNL Hydride Databases.
21. R. Bau, D. M. Ho, and S. G. Gibbins, *J. Am. Chem. Soc.*, 1981, **103**, 4960; see also D. E. Linn Jr, G. M. Skidd, and E. M. Tippmann, *Inorg. Chim. Acta*, 1999, **291**, 142.
22. R. G. Teller and R. Bau, *Struct. Bonding (Berlin)*, 1981, **44**, 1; see also R. Bau, M. Y. Chiang, D. M. Ho, S. G. Gibbins, T. J. Emge, and T. F. Koetzle, *Inorg. Chem.*, 1984, **23**, 2823.
23. K. Yvon and P. Fischer, *Top. Appl. Phys.*, 1988, **63**, 87 (Springer).
24. W. Bronger, L. à Brassard, P. Müller, B. Lebeck, and Th. Schultz, *Z. Anorg. Allg. Chem.*, 1999, **625**, 1143.
25. R. Lindsay, R. O. Moyer, J. S. Thompson, and D. Kuhn, *Inorg. Chem.*, 1976, **15**, 3050; see also R. Lindsay and R. O. Moyer Jr, *Inorg. Chem.*, 1981, **80**, P37; see also R. O. Moyer Jr, R. Lindsay, and D. F. Storey, *Z. Phys. Chem. Neue Folge*, 1989, **165**, 83; see also R. Lindsay, R. O. Moyer, W. Strange, W. H. Klapp, D. F. Storey, and J. R. Knapp, *Z. Phys. Chem. Neue Folge*, 1993, **179**, 457; for Eu_2IrH_5 see R. O. Moyer Jr and R. Lindsay, *J. Less-Common Met.*, 1980, **70**, P57.
26. J.-J. Didisheim, P. Zolliker, K. Yvon, P. Fischer, J. Schefer, M. Gubelmann, and A. F. Williams, *Inorg. Chem.*, 1984, **23**, 1953.
27. M. Kritikos, D. Noréus, B. Bogdanovic, and U. Wilczok, *J. Less-Common Met.*, 1990, **161**, 337.
28. M. Kritikos and D. Noréus, *J. Solid State Chem.*, 1991, **93**, 256.
29. B. Huang, F. Bonhomme, P. Selvam, K. Yvon, and P. Fischer, *J. Less-Common Met.*, 1991, **171**, 301.
30. P. Selvam and K. Yvon, *Int. J. Hydrogen Energy*, 1991, **16**, 615.
31. J. Huot, H. Hayakawa, and E. Akiba, *J. Alloys Comp.*, 1997, **248**, 164; see also J. Huot, S. Boily, E. Akiba, and R. Schulz, *J. Alloys Comp.*, 1998, **280**, 306.

32. A. Hightower, B. Fultz, and R. C. Bowman Jr, *J. Alloys Comp.*, 1997, **252**, 238; see also S. S. Sai Raman, D. J. Davidson, J.-L. Bobet, and O. N. Srivastava, *J. Alloys Comp.*, 2002, **333**, 282; see also F. C. Gennari, F. J. Castro, and J. J. A. Gamboa, *J. Alloys Comp.*, 2002, **339**, 261.
33. W. Bronger and G. Auffermann, *Angew. Chem., Int. Ed. Engl.*, 1994, **33**, 1112.
34. W. Bronger and G. Auffermann, *J. Alloys Comp.*, 1995, **219**, 45.
35. W. Bronger and G. Auffermann, *Z. Anorg. Allg. Chem.*, 1995, **621**, 1318.
36. J. S. Thompson, R. O. Moyer, and R. Lindsay, *Inorg. Chem.*, 1975, **14**, 1866; see also R. Lindsay, R. O. Moyer Jr, W. Strange, and B. J. Burnim, *J. Alloys Comp.*, 1996, **243**, 90; for Yb₂RuH₆ see R. Lindsay, R. O. Moyer Jr, J. S. Thompson, and D. Kuhn, *Inorg. Chem.*, 1976, **15**, 3050.
37. E. Orgaz and M. Gupta, *Z. Phys. Chem.*, 1993, **181**, 1; see also M. Gupta and L. Schlapbach, *Top. Appl. Phys.*, 1988, **63**, 139; see also M. Gupta, *J. Less-Common Met.*, 1984, **103**, 325.
38. S. F. Parker, K. P. J. Williams, M. Bortz, and K. Yvon, *Inorg. Chem.*, 1997, **36**, 5218.
39. B. Bogdanovic, A. Reiser, K. Schlichte, B. Spliethoff, and B. Tesche, *J. Alloys Comp.*, 2002, **345**, 77.
40. R. O. Moyer Jr, J. R. Wilkins, and P. Ryan, *J. Alloys Comp.*, 1999, **290**, 103.
41. J. Zhuang, J. M. Hastings, L. M. Corliss, R. Bau, C.-Y. Wei, and R. O. Moyer Jr, *J. Solid State Chem.*, 1981, **40**, 352.
42. J. Zhuang, W. Kunmann, L. M. Corliss, J. M. Hastings, and R. O. Moyer Jr, *J. Solid State Chem.*, 1983, **48**, 117; for Ca₂IrD₅ see R. O. Moyer Jr and B. H. Toby, *J. Alloys Comp.*, 2004, **363**, 99.
43. H. Kohlmann, R. O. Moyer, T. Hansen, and K. Yvon, *J. Solid State Chem.*, 2003, **174**, 35.
44. P. Zolliker, K. Yvon, P. Fischer, and J. Schefer, *Inorg. Chem.*, 1985, **24**, 4177.
45. M. Yoshida, F. Bonhomme, K. Yvon, and P. Fischer, *J. Alloys Comp.*, 1993, **190**, L45.
46. W. Bronger, K. Jansen, and L. Breil, *Z. Anorg. Allg. Chem.*, 1998, **624**, 1477.
47. W. Bronger, R. Beissmann, and G. Ridder, *J. Alloys Comp.*, 1994, **203**, 91.
48. F. Bonhomme, P. Selvam, M. Yoshida, K. Yvon, and P. Fischer, *J. Alloys Comp.*, 1992, **178**, 167.
49. R. O. Moyer Jr, B. J. Burnim, and R. Lindsay, *J. Solid State Chem.*, 1996, **121**, 56.
50. W. Bronger, P. Müller, D. Schmitz, and H. Spittank, *Z. Anorg. Allg. Chem.*, 1984, **516**, 35.
51. K. Kadir, M. Kritikos, D. Noréus, and A. F. Andresen, *J. Less-Common Met.*, 1991, **172–174**, 36.
52. M. Gupta, *Z. Phys. Chem.*, 1993, **181**, 9.
53. W. Bronger and G. Auffermann, *J. Alloys Comp.*, 1995, **228**, 119.
54. S. F. Parker, K. P. J. Williams, T. Smith, M. Bortz, B. Bertheville, and K. Yvon, *Phys. Chem. Chem. Phys.*, 2002, **4**, 1732.
55. U. Häussermann, H. Blomqvist, and D. Noréus, *Inorg. Chem.*, 2002, **41**, 3684.
56. P. Zolliker, K. Yvon, and C. Baerlocher, *J. Less-Common Met.*, 1986, **115**, 65; see also D. Noréus and L. Kihlberg, *J. Less-Common Met.*, 1986, **123**, 233.
57. K. Yvon, J. Schefer, and F. Stucki, *Inorg. Chem.*, 1981, **20**, 2776.
58. E. Rönnebro, J. O. Jensen, D. Noréus, and N. J. Bjerrum, *J. Alloys Comp.*, 1999, **293–295**, 146.
59. W. Bronger, G. Auffermann, and P. Müller, *J. Less-Common Met.*, 1986, **116**, 9; see also W. Bronger, G. Auffermann, and P. Müller, *J. Less-Common Met.*, 1988, **142**, 243; see also W. Bronger, and G. Auffermann, *J. Alloys Comp.*, 1992, **187**, 87.
60. D. Noréus, K. W. Törnroos, A. Börje, T. Szabó, W. Bronger, H. Spittank, G. Auffermann, and P. Müller, *J. Less-Common Met.*, 1988, **139**, 233; see also K. Kadir and D. Noréus, *Z. Phys. Chem. NF.*, 1989, **163**, 231.
61. R. V. Kasowski, D. Noréus, L. Wang, and M.-H. Whangbo, *Inorg. Chem.*, 1992, **31**, 4737.
62. W. Bronger and G. Auffermann, *J. Less-Common Met.*, 1991, **169**, 173.
63. W. Bronger, G. Auffermann, and P. Müller, *Z. Anorg. Allg. Chem.*, 1988, **566**, 31; see also W. Bronger and G. Auffermann, *J. Alloys Comp.*, 1992, **187**, 81; W. Bronger and G. Auffermann, *J. Alloys Comp.*, 1992, **179**, 235.
64. W. Bronger and G. Auffermann, *J. Less-Common Met.*, 1990, **158**, 163.
65. W. Bronger, K. Jansen, and P. Müller, *J. Less-Common Met.*, 1990, **161**, 299.
66. B. Huang, Synthèse, Structure et Stabilité Thermique des Hydrures Ternaires et Quaternaires Complexes des Métaux de Transition, Thesis No 2765 (in English), University of Geneva, 1995.
67. W. Bronger and G. Ridder, *J. Alloys Comp.*, 1994, **210**, 53.
68. H. Kohlmann, H. E. Fischer, and K. Yvon, *Inorg. Chem.*, 2001, **40**, 2608; see also K. H. J. Buschow, R. L. Cohen, and K. W. West, *J. Appl. Phys.*, 1977, **48**, 5289.
69. K. Ensslen, E. Bucher, and H. Oesterreicher, *J. Less-Common Met.*, 1983, **92**, 343.
70. H. T. Takeshita, T. Oishi, and N. Kuriyama, *J. Alloys Comp.*, 2002, **333**, 266.
71. E. Orgaz, V. Mazel, and M. Gupta, *J. Alloys Comp.*, 1997, **253–254**, 330.

72. M. Kritikos, D. Noréus, A. F. Andresen, and P. Fischer, *J. Solid State Chem.*, 1991, **92**, 514.
73. W. Bronger, M. Gehlen, and G. Auffermann, *J. Alloys Comp.*, 1991, **176**, 255.
74. W. Bronger, P. Müller, J. Kowalczyk, and G. Auffermann, *J. Alloys Comp.*, 1991, **176**, 263.
75. W. Bronger, M. Gehlen, and G. Auffermann, *Z. Anorg. Allg. Chem.*, 1994, **620**, 1983.
76. L. B. Lundberg, D. T. Cromer, and C. B. Magee, *Inorg. Chem.*, 1972, **11**, 400.
77. F. Bonhomme, K. Yvon, and P. Fischer, *J. Alloys Comp.*, 1992, **186**, 209; erratum, F. Bonhomme, K. Yvon, and P. Fischer, *J. Alloys Comp.*, 1992, **190**, 141; see also F. Bonhomme, Synthèse et Caractérisation Structurale d'Hydrures Ternaires Contenant du Magnésium et un Métal de Transition du Groupe VIII, Thesis No 2720 (in French), University of Geneva, 1995.
78. F. Bonhomme, K. Yvon, and P. Fischer, *J. Alloys Comp.*, 1992, **186**, 309.
79. B. Huang, K. Yvon, and P. Fischer, *J. Alloys Comp.*, 1992, **187**, 227; see also Huang, K. Yvon, and P. Fischer, *J. Alloys Comp.*, 1995, **227**, 121.
80. R. Černý, F. Bonhomme, K. Yvon, P. Fischer, P. Zolliker, D. E. Cox, and A. Hewat, *J. Alloys Comp.*, 1992, **187**, 233.
81. E. J. Ivanov, I. Konstanchuk, A. Stepanov, Yan. Jie, M. Pezat, and B. Darriet, *Inorg. Chem.*, 1989, **28**, 613; see also I. G. Konstanchuk, E. Yu. Ivanov, A. A. Stepanov, and T. I. Samsonova, *Izv. Akad. Nauk SSSR, Ser. Khim. Nauk*, 1989, **3**, 93 (in Russian).
82. F. Bonhomme, K. Yvon, G. Triscone, K. Jansen, G. Auffermann, P. Müller, W. Bronger, and P. Fischer, *J. Alloys Comp.*, 1992, **178**, 161.
83. B. Huang, K. Yvon, and P. Fischer, *J. Alloys Comp.*, 1992, **178**, 173; see also B. Huang, K. Yvon, and P. Fischer, *J. Alloys Comp.*, 1994, **204**, L5.
84. F. Gingl and K. Yvon, *Z. Kristallogr.*, 1993, **207**, 247.
85. B. Huang, K. Yvon, and P. Fischer, *J. Alloys Comp.*, 1992, **190**, 65; see also B. Huang, K. Yvon, and P. Fischer, *J. Alloys Comp.*, 1993, **197**, 65.
86. K. Kadir and D. Noreus, *Z. Phys. Chem.*, 1993, **179**, 237.
87. M. Yoshida, K. Yvon, and P. Fischer, *J. Alloys Comp.*, 1993, **194**, L11.
88. B. Huang, K. Yvon, and P. Fischer, *J. Alloys Comp.*, 1993, **197**, 97.
89. M. Bortz, B. Bertheville, K. Yvon, E. A. Movlaev, V. N. Verbetzky, and F. Fauth, *J. Alloys Comp.*, 1998, **279**, L8.
90. E. Orgaz and M. Gupta, *J. Alloys Comp.*, 1999, **330–332**, 323.
91. F. Bonhomme, N. T. Stetson, K. Yvon, P. Fischer, and A. W. Hewat, *J. Alloys Comp.*, 1993, **200**, 65.
92. W. Bronger, K. Jansen, and G. Auffermann, *J. Alloys Comp.*, 1993, **199**, 47.
93. W. Bronger and L. Breil, *Z. Anorg. Allg. Chem.*, 1998, **624**, 1819.
94. B. Huang, K. Yvon, and P. Fischer, *J. Alloys Comp.*, 1994, **210**, 243.
95. B. Huang, P. Fischer, and K. Yvon, *J. Alloys Comp.*, 1996, **245**, L24.
96. A. P. Ginsberg and C. R. Sprinkle, *Inorg. Synth.*, 1972, **13**, 219, and references therein.
97. N. T. Stetson, K. Yvon, and P. Fischer, *Inorg. Chem.*, 1994, **33**, 4598.
98. E. Orgaz and M. Gupta, *J. Alloys Comp.*, 1999, **293–295**, 217.
99. M. Bortz, K. Yvon, and P. Fischer, *J. Alloys Comp.*, 1994, **216**, 39.
100. M. Bortz, A. Hewat, and K. Yvon, *J. Alloys Comp.*, 1997, **248**, L1.
101. M. Olofsson-Martensson, M. Kritikos, and D. Noréus, *J. Am. Chem. Soc.*, 1999, **121**, 10908.
102. H. Kohlmann, H. E. Fischer, and K. Yvon, *Inorg. Chem.*, 2001, **40**, 2608.
103. E. Orgaz, *J. Alloys Comp.*, 2003, **356–357**, 191.
104. M. Bortz, K. Yvon, and P. Fischer, *J. Alloys Comp.*, 1994, **216**, 43.
105. M. Bortz, A. Hewat, and K. Yvon, *J. Alloys Comp.*, 1997, **253–254**, 13.
106. W. Bronger, S. Hasenberg, and G. Auffermann, *Z. Anorg. Allg. Chem.*, 1996, **622**, 1145.
107. W. Bronger, S. Hasenberg, and G. Auffermann, *J. Alloys Comp.*, 1997, **257**, 75.
108. M. Bortz, M. Gutmann, and K. Yvon, *J. Alloys Comp.*, 1999, **285**, L19.
109. K. Kadir and D. Noréus, *J. Alloys Comp.*, 1994, **209**, 213.
110. B. Huang, K. Yvon, and P. Fischer, *J. Alloys Comp.*, 1995, **227**, 116.
111. N. T. Stetson and K. Yvon, *J. Alloys Comp.*, 1995, **223**, L4.
112. W. Bronger and L. à Brassard, *Angew. Chem., Int. Ed. Engl.*, 1995, **34**, 898.
113. B. Huang, F. Fauth, and K. Yvon, *J. Alloys Comp.*, 1996, **244**, L1.
114. W. Bronger and L. à Brassard, *Z. Anorg. Allg. Chem.*, 1996, **622**, 462.
115. B. Huang, F. Gingl, F. Fauth, A. Hewat, and K. Yvon, *J. Alloys Comp.*, 1997, **248**, 13.
116. M. Olofsson, M. Kritikos, and D. Noréus, *Inorg. Chem.*, 1998, **37**, 2900.
117. W. Bronger, G. Auffermann, and H. Schilder, *Z. Anorg. Allg. Chem.*, 1998, **624**, 497.

118. W. Bronger and G. Auffermann, *Z. Anorg. Allg. Chem.*, 1999, **625**, 1147.
119. G. Auffermann, W. Bronger, R. M. Ibberson, and S. Hull, ISIS Facility Annual Report 2001–2002 – Highlights of ISIS Science, 2002, 22.
120. W. Bronger, T. Sommer, G. Auffermann, and P. Müller, *J. Alloys Compd.*, 2002, **330–332**, 536.
121. R. Cerny, J. M. Joubert, H. Kohlmann, and K. Yvon, *J. Alloys Comp.*, 2002, **340**, 180; see also R. Cerny, J. M. Joubert, and K. Yvon, *Mater. Sci. Forum*, 1998, **278–281**, 121.
122. L. Guénée, V. Favre-Nicolin, and K. Yvon, *J. Alloys Compd.*, 2003, **348**, 129.
123. G. Renaudin, L. Guénée, and K. Yvon, *J. Alloys Comp.*, 2003, **350**, 145.
124. D. M. P. Mingos, and J. C. Hawes, *Struct. Bonding (Berlin)*, 1985, **63**, 1; see also R. Hoffmann, *Angew. Chem., Int. Ed. Engl.*, 1982, **21**, 711.
125. K. Kadir, and D. Noréus, *Z. Phys. Chem.*, 1993, **179**, 249; see also K. Kadir, P. Lundqvist, D. Noréus, and O. Rapp, *Solid State Commun.*, 1993, **85**, 891.
126. B. Nacken and W. Bronger, *Z. Anorg. Allg. Chem.*, 1978, **439**, 29.
127. J. D. Corbett, *J. Solid State Chem.*, 1981, **39**, 56.
128. K. Yvon, H. Kohlmann, and B. Bertheville, *Chimia*, 2001, **55**, 505.
129. R. H. Crabtree, *Acc. Chem. Res.*, 1990, **23**, 95.
130. R. Griessen, *Europhys. News*, 2001, **32**, 41.
131. R. Griessen and T. Riesterer, *Top. Appl. Phys.*, 1988, **63**, 219.

Acknowledgment

The work was supported by the Swiss National Science Foundation and the Swiss Federal Office of Energy.